BRNO UNIVERSITY OF TECHNOLOGY
VYSOKÉ UČENÍ TECHNICKÉ V BRNĚ

FACULTY OF MECHANICAL ENGINEERING
FAKULTA STROJNÍHO INŽENÝRSTVÍ

INSTITUTE OF PHYSICAL ENGINEERING
ÚSTAV FYZIKÁLNÍHO INŽENÝRSTVÍ

DESIGN OF OPTOMECHANICAL MODULE FOR CHEMICAL MAPPING USING LASER-INDUCED BREAKDOWN SPECTROSCOPY

NÁVRH OPTOMECHANICKÉHO MODULU PRO CHEMICKÉ MAPOVÁNÍ METODOU SPEKTROSKOPIE LASEREM BUZENÉHO PLAZMATU

MASTER'S THESIS
DIPLOMOVÁ PRÁCE

AUTHOR
AUTOR PRÁCE

Bc. Anna Švábíková

ADVISOR
VEDOUCÍ PRÁCE

Ing. Pavel Pořízka, PhD.

BRNO 2019

BRNO UNIVERSITY OF TECHNOLOGY
FACULTY OF MECHANICAL ENGINEERING

Master's Thesis Assignment

Institut:	Institute of Physical Engineering
Student:	**Bc. Anna Švábíková**
Degree programm:	Applied Sciences in Engineering
Branch:	Physical Engineering and Nanotechnology
Supervisor:	**Ing. Pavel Pořízka, Ph.D.**
Academic year:	2018/19

As provided for by the Act No. 111/98 Coll. on higher education institutions and the BUT Study and Examination Regulations, the director of the Institute hereby assigns the following topic of Master's Thesis:

Design of optomechanical module for chemical mapping using Laser-Induced Breakdown Spectroscopy

Brief description:

Forensic analysis represents a field of study where it is possible to fully use advantages of the Laser-induced Breakdown Spectroscopy (LIBS) method. In the case of braking tracks detection, the investigative work is made difficult by the presence of current ABS systems, where no visually detectable braking tracks are created. Instead, braking tracks (made by a car with ABS system) leave only trace amounts of tyre's material that sticks to the road's surface. The length of the braking tracks then can be inspected with the help of characteristic signal of zinc, which is present in the mixture used for tyres' production.

The subject of this diploma thesis is mechanical design of optomechanical module, which will be implemented in a unique device designed for the application of braking tracks detection. This module will allow two-axis scanning of the road surface by the Laser-induced Breakdown Spectroscopy method. The output of the measurement will be an elemental map of the sample surface; i.e. the distribution of zinc determining the trajectory of the braking track on the road. The solution will allow i) the laser to be guided and focused on the surface and ii) to collect plasma radiation that will be led by the collecting optics to the detector. As an output of this thesis is a complete production documentation.

Master's Thesis goals:

1. Review of LIBS literature regarding in-situ analysis and design of compact LIBS devices.
2. Conceptual designs of optical path and evaluation of individual options.
3. Design of LIBS module and creation of production documentation.

Recommended bibliography:

MIZIOLEK, A. W., PALLESCHI, V. and SCHECHTER, I. Laser Induced Breakdown Spectroscopy. 1st edition. Cambridge: Cambridge University Press, 2006. ISBN 978-051-1541-261.

GLÉZL, Š., SLIMÁK, I. and KAMARÁD, J. Presná mechanika. Bratislava: Alfa, 1992. ISBN 80-050-0972-0.

Students are required to submit the thesis within the deadlines stated in the schedule of the academic year 2018/19.

In Brno, 26. 10. 2018

VYSOKÉ UČENÍ TECHNICKÉ V BRNĚ FAKULTA STROJNÍHO INŽENÝRSTVÍ DĚKANÁT 11

prof. RNDr. Tomáš Šikola, CSc.
Director of the Institute

doc. Ing. Jaroslav Katolický, Ph.D.
FME dean

ABSTRACT

This diploma thesis deals with the design of an optomechanical module for chemical mapping using the Laser-Induced Breakdown Spectroscopy (LIBS) method. The main goal is to develop a module capable of the analysis of zinc spectral lines in the ultraviolet (UV) region. Basic theory of the LIBS method is described in this work, followed by a research focusing on the remote LIBS analysis. Possible optical designs of focusing and collecting optics are presented in this work. Chosen optical designs were then tested. The output of this work is the final optomechanical design of the module.

KEYWORDS

Laser-Induced Breakdown Spectroscopy (LIBS), optomechanical design, remote analysis

ABSTRAKT

Tato diplomová práce se zabývá návrhem optomechanického modulu pro chemické mapování metodou spektroskopie laserem buzeného plazmatu (LIBS). Cílem je vyvinout modul, který bude umožňovat analýzu spektrálních čar zinku v ultrafialové (UV) oblasti. V práci jsou popsány teoretické základy metody LIBS a následně je provedena rešerše zaměřená na problematiku dálkové LIBS analýzy. V diplomové práci jsou prezentovány možné optické návrhy fokusační a sběrné optiky, z nichž jsou vybrané následně otestovány. Výsledkem práce je konstrukční návrh modulu.

KLÍČOVÁ SLOVA

spektroskopie laserem buzeného plazmatu (LIBS), optomechanický návrh, dálková analýza

ŠVÁBÍKOVÁ, Anna. *Design of optomechanical module for chemical mapping using Laser-Induced Breakdown Spectroscopy*. Brno, 2019, 94 p. Master's Thesis. Brno University of Technology, Faculty of Mechanical Engineering, Institute of Physical Engineering. Advised by Ing. Pavel Pořízka, PhD.

DECLARATION

I declare that I have written the Master's Thesis titled "Design of optomechanical module for chemical mapping using Laser-Induced Breakdown Spectroscopy" independently, under the guidance of the advisor and using exclusively the technical references and other sources of information cited in the thesis and listed in the comprehensive bibliography at the end of the thesis.

As the author I furthermore declare that, with respect to the creation of this Master's Thesis, I have not infringed any copyright or violated anyone's personal and/or ownership rights. In this context, I am fully aware of the consequences of breaking Regulation § 11 of the Copyright Act No. 121/2000 Coll. of the Czech Republic, as amended, and of any breach of rights related to intellectual property or introduced within amendments to relevant Acts such as the Intellectual Property Act or the Criminal Code, Act No. 40/2009 Coll., Section 2, Head VI, Part 4.

Brno ....

author's signature

ACKNOWLEDGEMENT

I would like to express my thanks to my supervisor Ing. Pavel Pořízka, Ph.D. I would also like to thank Ing. David Prochazka, Phd. for his factual comments and guidance through my experimental work and Ing. Jan Novotný, Ph.D for his advices in the field of optical design. I would like to acknowledge the support of CEITEC Nano Research Infrastructure, particularly Ing. Josef Polčák, Ph.D for performing the XPS analysis. Last but not least, I would like to thank Bc. František Hlaváč for his support and patience during my work on this diploma thesis.

Brno . . . .

author's signature

Contents

Introduction

Laser-Induced Breakdown Spectroscopy (LIBS) is a relatively young method of atomic emission spectroscopy. Laser induced plasma was first observed shortly after the invention of pulsed ruby laser by Theodore Maiman in 1960. However, the potential of LIBS method remained dormant until 1980s and a true boom of the method came in the first decade of the 21st century [1]. Over the last three decades, LIBS has become a promising and widely researched field.

Nowadays, LIBS method is mostly used for research purposes. Commercial and industrial applications are still rather scarce. Nevertheless, LIBS is very variable in its usage and its applications cover a broad spectrum of fields of study (e.g. detection of explosives [2], structural analysis of paintings [3], food analysis [4], scrap metal classification [5], forensic analysis [6], etc.). However, the true potential of the method lies in remote and in-situ applications.

If an object is about to be analysed in laboratory conditions, the sample needs to be collected, physically transported to the laboratory and usually also pre-treated. This process may be lengthy and expensive and in some cases even impossible. For this reason, research groups are focusing on mobile applications of various spectroscopic methods. Many devices were developed during the last decades, using methods like GC-MS (Gas Chromatography – Mass Spectrometry), XRF (X-ray Fluorescence) [7], Raman Spectroscopy [8] or IMS (Ion Mobility Spectrometry) [9]. LIBS had been able to establish its position among conventional methods. Reasons why LIBS appeared as an ideal candidate were simple – the principle of LIBS allows to construct robust and relatively simple devices. LIBS analysis is rapid, inexpensive and almost non-destructive. One of the biggest advantages is that, in most cases, a sample does not need any pre-treatment. This would enable an analysis of dangerous samples or samples with limited accessibility without the need of physical access the sample.

Table 1 shows some of the most important features of different analytical techniques mentioned above related to field analysis. It is obvious that no perfect technique offering all analytical capabilities exists and the choice depends on requirements and preferences of the specific application. For some applications it is not uncommon to combine two analytical techniques like LIBS/Raman or LIBS/LIF [1] in order to obtain better results [10]. Conventional techniques have been already successfully implemented into real-word applications. However, the use of the field

[1]LIF = Laser-induced Fluorescence

LIBS devices is enjoying the growth in popularity with an ambition to successfully enter the market with its relatively affordable and easy-to-operate instruments.

Tab. 1: Comparison of different analytical techniques. The rating is illustrated by stars - the more stars, the better performance. Data were taken from [10]

	LIBS	CG-MS	Raman	IMS	XRF
Analytical Capabilities					
Selectivity	***	*****	****	**	***
Detection Power	**	*****	***	**	***
Absolute Analysis	**	*****	*****	**	**
Analytical Information	atomic	molecular	molecular	molecular	atomic
Operational Features					
Sample Preparation	*****	*****	*****	*****	*****
Sample Size	*****	*****	*****	*****	*****
Lateral Resolution	****	-	***	-	**
Depth Resolution	*****	-	-	-	-
Speed	*****	*****	****	***	***
Simplicity of Analysis	****	****	****	****	****
Solid Sampling Capacity	*****	-	*****	-	*****
Instrumentation Maturity	**	****	***	***	***

LIBS devices for in-situ measurements typically come in two basic arrangements, so called *remote* LIBS and *stand-off* LIBS arrangement. The difference between these two lies in the means of signal transfer. While the signal is transferred by optical cables in remote LIBS, stand-off LIBS uses the air as a transfer medium. The basics of LIBS instrumentation for in-situ analysis are summarized in several review articles (e.g.[10, 11]). Undoubtedly, the most famous application of LIBS is the ChemCam, which is a part of Curiosity rover. Nevertheless, due to the technical advancement, more and more applications of remote LIBS appear in fields, where in-situ and rapid analysis is needed.

One of many applications where the potential of the LIBS method may be fully employed is the forensic analysis of braking tracks. This topic was opened by Dr. Prochazka from Brno University of Technology in his dissertation thesis [12] and publications [6, 13]. LIBS could be effectively used for fast and convenient analysis of otherwise visually non-recognizable braking tracks. The problem in the determination of braking tracks (their presence or absence) is closely related to goals of this diploma thesis which aims to introduce a device for a braking tracks analysis.

1 Laser-induced Breakdown Spectroscopy

A great advantage of the LIBS method is its relatively simple and low-cost instrumentation. Typical LIBS instrumentation, needed for a basic laboratory experiment, is shown in Fig. 1.1. For most of LIBS applications, Q-switched Nd:YAG pulsed lasers are used. The energy of the pulse is typically in tens or hundreds of mJ. Laser pulse is then focused by the focusing lens in a small spot (hundreds of µm) on the sample surface. By focusing the sample, the irradiation on the sample can reach very high ($GW \cdot cm^{-2}$) values. Laser beam induces the creation of plasma plume (the process itself is described in section 1.2) and the radiation of the plume is led by collecting optics to a slit of a spectrometer. Collecting optics can consist of system of achromatic lenses, however, the usage of reflective optics has more advantages especially for remote applications. The output from the spectrometer is a spectrum of spectrally resolved lines, which are then detected by a detector (CCD, ICCD, etc.).

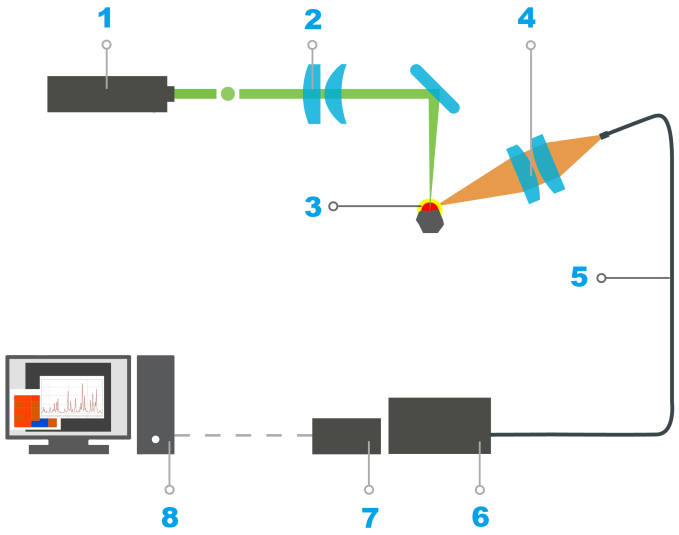

Fig. 1.1: Typical LIBS instrumentation. Laser pulse generated by the laser head (1) is focused by focusing optics (2) on the sample surface (3). Radiation of the plasma, induced on the sample surface, is focused by the collecting optics (4) on the optical fiber (5). The fiber leads the signal into the spectrometer (6) where it is dispersed and captured by a detector (7). Resulting spectra are then displayed on the PC (8). Taken from [14] and edited.

The laser-matter interaction is a complex phenomenon linked with multiple physical and chemical processes. When simplified, the mechanism of the interaction can be divided into following three steps [12]:

- heating and melting of the sample,
- ablation,
- ionisation and optical breakdown.

Although this chapter does not fully describe the interaction of the laser with a sample, it aims to deliver a basic introduction into the matter.

1.1 Lasers in LIBS

The choice of laser is crucial because it directly determines the nature of whole experiment. Main parameters, relevant to LIBS, are energy and its stability, pulse width, wavelength and repetition rate [15, 16]. Another important parameter is irradiance, depending on the laser pulse energy, width and the spot diameter created by focusing the laser beam on the sample surface.

The energy of the laser radiation determines the energy available for the whole mechanism of plasma generation. Energies of a typical laser pulse lie in the range from 1 to 1000 mJ [16]. A parameter directly linked with the pulse energy is the irradiance. For the generation of plasma, an above-threshold irradiance is needed. By focusing the laser pulse with the focusing lenses a high irradiance ($GW \cdot cm^{-2}$) is achieved on the sample surface, providing enough energy for the mechanism of plasma generation.

Pulse width can alter the result of an experiment by changing the process of plasma ablation. In LIBS, either nanosecond or femtosecond pulsed lasers are used. Lasers with nanosecond pulses are more common, however, more and more experiments with femtosecond lasers appear. For nanosecond pulses (typically 10-20 ns [16]), the energy from the laser radiation is thermally transferred to the sample. Plasma is generated and evolves while the laser radiation persists, which means that the plasma is affected by the pulse [17]. When using fs pulses, the energy from the laser radiation is transferred by the mechanism of Coulomb explosion. The gradual heating and melting of the sample, present when using ns pulses, does not occur. Instead the Coulomb force between electron and ionised atoms causes the tearing of chemical bonds, leading to generation of a plasma plume [18].

In the majority of LIBS experiments, the most widely used are Nd:YAG lasers. The fundamental wavelength of the laser is 1064 nm, higher harmonics are 532, 366 or 266 nm. Wavelength of the laser radiation determines the portion of pulse energy that is absorbed by the material. This parameter determines the optical

penetration depth – the depth in sample where laser irradiance decreases to 37 % of initial value. The penetration depth rises with wavelength of the laser radiation [16].

Last parameter mentioned is repetition rate. Repetition rate defines the maximum frequency of laser pulses. Most of the time when using ns pulsed lasers, high frequency is usually not appropriate and ranges in tens of Hz. This parameter becomes crucial especially for spatially resolved analysis and femtosecond pulsed lasers where higher repetition rates are needed [19].

1.2 Laser-induced Plasma

The laser pulse incident on the sample surface has high irradiance (up to hundreds of $GW \cdot cm^{-2}$ [18]). Fraction of the laser energy is absorbed by the sample material when the photons collide with atoms and molecules in the sample. This leads to the release of free electrons from the sample. The rest of the energy contributes to heating and consecutively to melting of the sample surface. After the material is locally heated to its melting point, it starts to evaporate. The temperature on the surface exceeds the melting temperature of all materials present in the sample. Thus, we can presume that intensities of elements present in the plasma are matching the real composition of the sample.
Because the temperature of the vapour is very high, we can also assume that there always exist some free electrons [16]. These free electrons absorb the energy of the pulse through the inverse Bremsstrahlung, thus get accelerated and collide with neutral atoms, molecules and photons in the vapour. By this mechanism an avalanche ionization occurs – so called optical breakdown. The energy needed for the optical breakdown depends on the material of the sample and on properties of the laser beam [12].

Plasma is defined as a local assembly of atoms, ions and free electrons that is quasineutral and that acts collectively. The quasineutrality of the plasma means that the concentration of positive and negative charges in certain area is roughly equal. The collective behaviour means that the plasma reacts to an external field as a whole and can generate fields. Plasma can be defined by a variety of parameters. Some of basic parameters are the degree of ionisation, frequency, electron density and temperature [12].

The laser-induced plasma (LIP) typically falls in the category of weakly ionised plasmas. This means that the ratio of electrons to other species is less than 10 %[20].

Because of the low degree of ionisation, the laser pulse is able to reach the sample surface. On the other hand, if the energy of the pulse is high, a thin partially ionised film is created between the surface and vapour and the laser pulse cannot reach the sample anymore. This occurs when the plasma frequency is higher than the laser pulse frequency or when the electron density of the ionised film exceeds a critical value given by [12]

$$n_c \approx \frac{10^{21}}{\lambda^2} \frac{1}{\mathrm{cm}^3}, \tag{1.1}$$

where λ is the wavelength of the laser beam in micrometres. The electron density is lowered again by absorption of the beam energy by the sample and the sample is opaque. This process repeats with every pulse.

In order to determine the basic parameters of plasma such as electron density and temperature, the system needs to be in thermodynamic equilibrium and optically thin. Being in a complete thermodynamic equilibrium means that all processes in plasma can be described by statistical mechanics and are characterized by a single temperature. In this state, each process in the plasma is balanced by its reverse process. In complete thermodynamic equilibrium, the system can be described by the Maxwellian distribution of energy and the atomic states have Boltzmann distribution[21].
Unfortunately, complete thermodynamic equilibrium is unachievable in LIP. To achieve complete thermodynamic equilibrium, the plasma ought to be optically thin at all frequencies. The real plasma's mass is expanding unevenly from its centre to its edges and the energy spread is inhomogenous. Also, a part of plasma energy is lost due to radiation. Therefore, to be able to determine parameters of a plasma, an approximation is needed. The energy losses due to radiation can be neglected compared to other processes in plasma and collisions - therefore we can assume that a complete thermodynamic equilibrium exists in small areas of the plasma. This way, plasma can be divided into areas in thermodynamic equilibriums and there does not need to be any connection in means of thermodynamic equilibrium between adjacent ones. This approximation is called Local Thermodynamic Equilibrium (LTE). LTE occurs if the electron density in plasma is high enough. Threshold value of the electron density is given by McWhirter's criterion

$$n_e \geq 1.6 \cdot 10^{12} T^{\frac{1}{2}} (\Delta E_{nm})^3, \tag{1.2}$$

where n_e (cm^{-3}) is electron density, T (K) plasma temperature and ΔE_{nm} (eV) is the energy difference between energy levels n and m [22]. However, McWhirther criterion is sufficient for a stationary and homogenous plasma, which does not consider spatial gradients and time-variation of the plasma. For a real plasma induced by laser

radiation, this criterion is considered as the condition necessary, but not sufficient. More information about criterions of LTE, including the models fitting the real plasma, can be found for example in [22].

1.3 Spectral Lines

Spectral lines are the representatives of each element present in the sample. They are the means of determining parameters of LIP and the analysis input for methods of atomic emission spectroscopy. Because an atom or molecule emits single photon at well-defined energy during its transition from one energy level to another, one might expect that the spectral line profiles are represented by Dirac distribution. However, due to the complicated physical phenomena, taking place in plasma, the shape of spectral lines is defined by its FWHM (full width at half maximum) parameter. The shape of the spectral line is determined by the dominant mechanism of broadening.

Natural broadening of spectral lines is due to the Heisenberg's principle of uncertainty. The finite lifetime of an excited state Δt and the energy of the state ΔE must satisfy the uncertainty equation

$$\Delta E \Delta t \geq \frac{h}{4\pi}. \tag{1.3}$$

The result of the natural broadening is Lorentz profile. For LIP, the effects of natural broadening can be neglected [20].

The Doppler broadening is a result of the movement of emitting particles. The Doppler broadening strongly depends on the plasma temperature and mass of emitting particles and reflects the kinetic energy of particles in the plasma. Measuring the Doppler broadening therefore allows the determination of plasma temperature [23]. The result of Doppler broadening is Gauss line profile.

Lorentz (or pressure) broadening is result of interactions between emitting atoms of the element considered and atoms of other elements [23]. Depending on the interaction, pressure broadening can be divided into three categories – van der Waals broadening (interaction with neutrals), resonant broadening (atoms or ions of same kind), and Stark broadening (interaction with charged particles). In laser spectroscopy, Stark broadening is the dominating mechanism, leading to the shift and broadening of spectral lines. The shift of lines peaks is caused by splitting of energy levels to sublevels according to the absolute value of the z-component of angular

momentum quantum number [20]. This leads to an uneven distribution of transitions between levels, causing the peak shifts.

In most of LIBS experiments, the profile of spectra is given by the combination of Doppler and Stark broadening. This results in the Voigt (or less compute intensive Pseudo-Voigt) profile of spectral lines, given by the convolution of Gauss and Lorentz profile. Even though other broadening mechanisms exist (e.g. instrumental or inhomogenous broadening), they are negligible in LIBS experiments. In Fig. 1.2 we can see the comparison between Gauss, Lorentz and pseudo-Voigt profile.

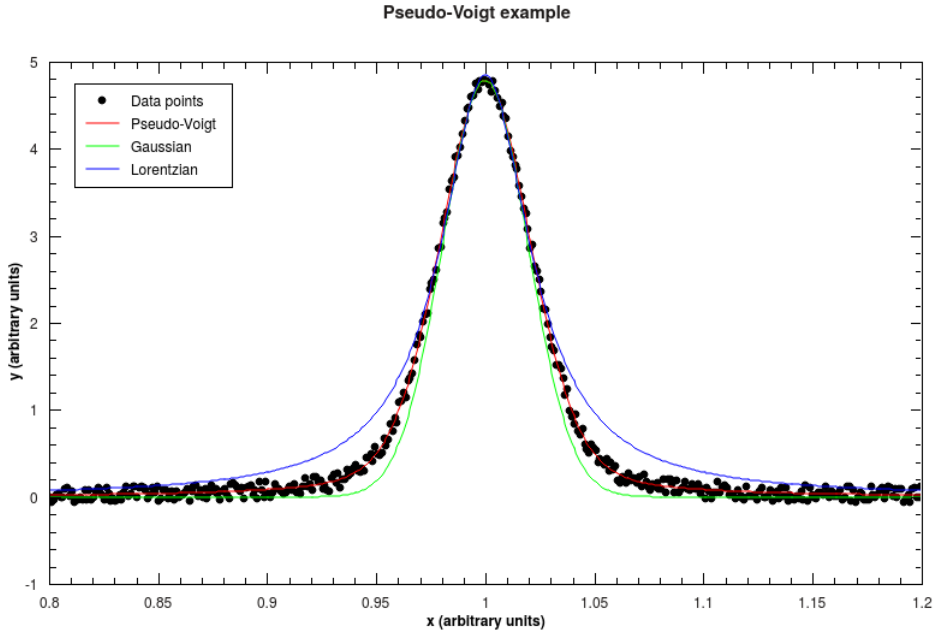

Fig. 1.2: Gauss and Lorentz profiles of equal FWHM and resulting Voigt profile. The y axis represents relative intensity, wavelength is plotted on the x axis. Taken from [24].

1.4 Determination of Plasma Parameters

The temperature and electron density of the plasma can be deduced experimentally (for example by a Langmuir probe [1]. However, in spectroscopy, LIP parameters are commonly determined by the means of spectral lines analysis. As was mentioned in section 1.2, LIP parameters can be determined with the assumption of LTE. When

[1]Langmuir probe is a device that serves for determining electron density, temperature and potential of the plasma. One or more electrodes are inserted into a plasma and by measuring currents and potentials in the system, properties of the plasma are determined.

the plasma is in LTE, the population density of certain species in excited quantum states n_k^s can be described by the Boltzmann distribution [25]:

$$n_k^s = n^s \frac{g_k}{U^s(T)} \exp\left(\frac{-E_k}{k_B T}\right), \tag{1.4}$$

where n^s (cm^{-3}) is the total number density of species s in LIP, g_k (-) statistical weight, $U_s(T)$ (-) internal partition function, E_k (eV) excitation energy of level k, k_B ($\mathrm{eV{\cdot}K^{-1}}$) Boltzmann constant and T (K) LIP temperature. Internal partition function of species s in LIP of temperature T is given by [25]:

$$U_s(T) = \sum_i g_i \exp\left(\frac{-E_i}{k_B T}\right). \tag{1.5}$$

The integral density I_λ^{ki} (in $\mathrm{cm^{-3}s^{-1}}$) of an optically thin emission line of wavelength λ in LIP can then be expressed as [25]:

$$I_\lambda^{ki} = A_{ki} n_k^s, \tag{1.6}$$

where A_{ki} is the transition probability (s^{-1}), or so called Einstein coefficient. With the knowledge of intensity of more lines of the same element, LIP temperature can be determined. Temperature of a plasma can be determined either by Boltzmann plot or Saha equation [26].

The Boltzmann plot method is derived from applying a natural logarithm into equation (1.6). The resulting line has a slope of $-1/k_B T$ and the temperature can be determined by using linear regression. It is an elegant way to determine the plasma temperature without the need of knowing plasma density. It is composed of multiple lines of the same element originating from different quantum transitions. The slope of Boltzmann plot is $\frac{-1}{k_B T}$, meaning that the temperature can be directly determined from linear regression [17]. An example of a Boltzmann plot is shown in Fig. 1.3.

The temperature acquired via Boltzmann plot method does not necessarily have to be accurate enough. A better (and more complicated) approach to plasma temperature measurements uses the fact that emission lines from different ionisation stages are usually present in a plasma. By the combination of Saha ionisation and Boltzmann distribution of plasma the temperature is given by the Saha-Boltzmann relation, defining the ionic/atomic emission radiance ratio. Applying natural logarithm to the Saha-Boltzmann relation and plotting the logarithmic ratios of several ionic and atomic emission lines as a function of their energy differences results in a line with a slope is inversely proportional to plasma temperature [26].

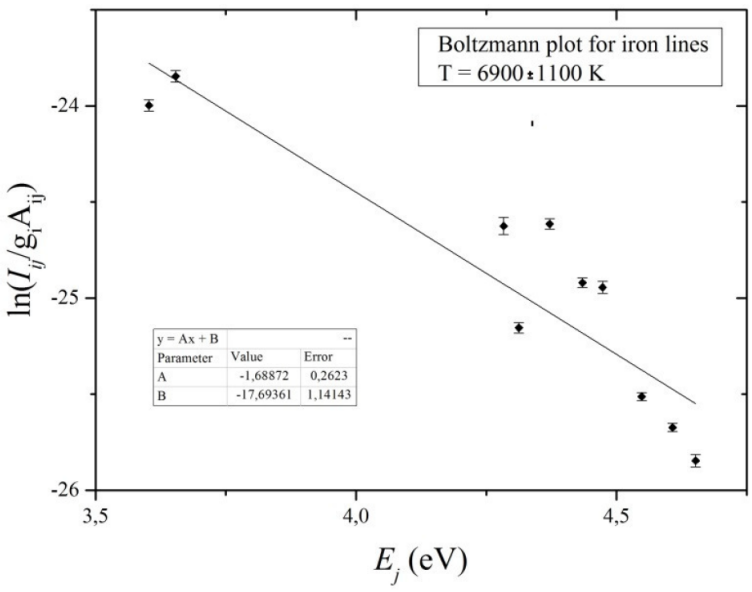

Fig. 1.3: Example of a Boltzmann plot based on atomic lines of iron [17].

Electron density n_e is commonly determined by two spectroscopic methods – either by measurement of Stark broadening of spectral lines or by measuring the population ratio of two successive ionisation states of a certain element.
As was mentioned above, the profile of LIBS spectral lines is given mostly by the Stark broadening. The value of Stark broadening coefficient can be calculated directly from the spectral lines profile. In LIBS, where the ion interactions and broadening can be neglected and the Stark broadening, expressed by the FWHM, is given by [26]

$$\Delta\lambda_{Stark} = 2w_e \left(\frac{n_e}{10^{16}}\right), \tag{1.7}$$

where w_e is the electron impact half-width, which value can be found in the literature. The electron density can be roughly determined from the relation (1.8).

1.5 Temporal Resolution of the LIBS spectra

Typical phenomenon in a laser-induced plasma is its rapid temporal evolution. During the laser pulse, the plasma grows in time and space. With the end of the pulse the plasma starts to decay, emitting the absorbed energy through deexcitations, electron recombination and Bremsstrahlung [27]. First, the background caused mainly by the Bremsstrahlung and recombination is dominant in the spectra and no spectral lines are visible. The background decays and in hundreds of ns, spectral lines start to be visible. The main goal is to find a compromise between the intensity of

spectral lines and the background - the signal-to-noise ratio (SNR). This is determined by the gate delay – the delay between the pulse and the detection.
Another important parameter is the exposition time (or gate width). This parameter characterises the length of detection which needs to be long enough to detect spectral lines and short enough not to capture too much noise.

For example, Porizka obtained a time-resolved spectrum in his dissertation thesis [17]. Each measured spectrum was obtained with the same gate width and was temporarily resolved by the gate delay (with a step of 100 ns). His results are shown in Figure 1.4. Because the temporal evolution is specific for every plasma, the optimum gate delay and spatial resolution have to be found for every species analysed.

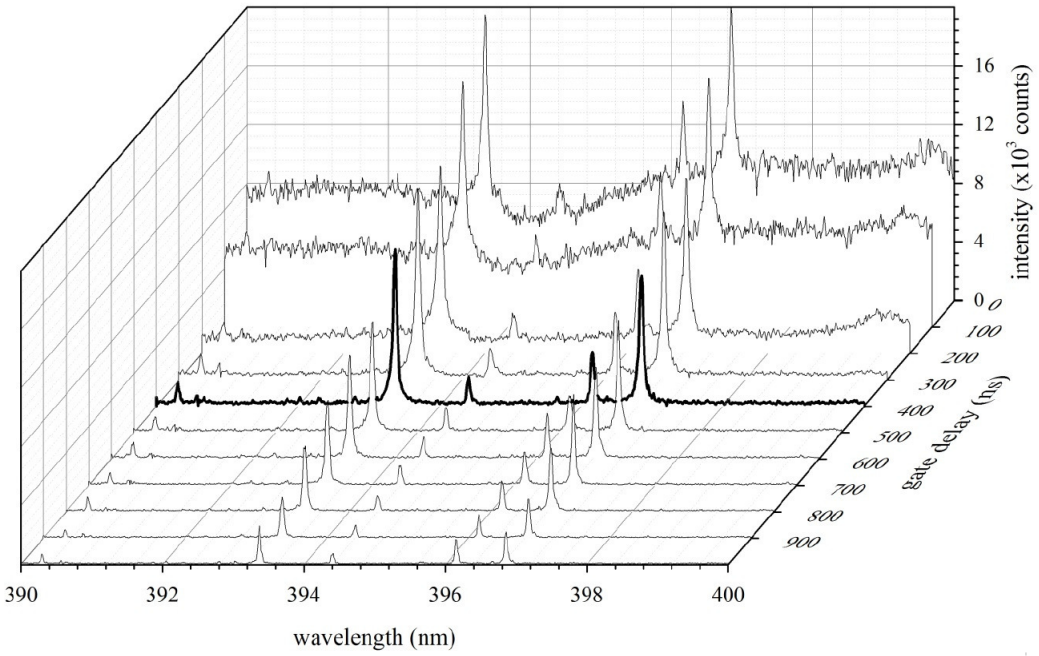

Fig. 1.4: Temporal resolution of a LIBS spectrum. The bold line shows the optimal gate delay according to the corresponding SNR [17].

1.6 Qualitative Analysis

Qualitative analysis represents a basic way of LIBS data analysis, based on determining the presence of an element in the sample. As was mentioned before, each spectral line is a characteristic of a certain element, specifically a certain transition between energy levels of an atom or an ion. The prime identification parameter of a

spectral line is its wavelength. Practically, this means that spectral line wavelengths of a measured spectrum are qualitatively compared with spectral line wavelengths listed in a database. In most cases, these databases can be accessed online (for example the NIST database [28]).

More than as an absolute tool, the spectral databases need to be taken as a starting point for spectral lines identification. For a correct analysis by comparing the spectral lines, a certain level of the operator's experience is needed. When evaluating spectral lines, several factors have to be taken into account, some of them being the relative intensity of the spectral line, Einstein coefficient, upper energy level of the transition, the degree of ionisation and expected composition of the sample. If a spectrum contains a line that could be classified in more ways, factors mentioned above are becoming crucial for the correct assignment. To name an example, if the radiation wavelength of a spectral line roughly corresponds to two lines in a database, one being an atomic line and the other one being once or more times ionised, it is very likely that the line is correctly classified as the first option, because the probability of transition from the atomic state is higher [12].

Because manual classification of spectral lines is a time-consuming and monotonous operation, several algorithms for automatic classification are being developed. One example for all is a commercially available AtomAnalyzer software [29], which is also used as a tool for spectra classification in this diploma thesis.

1.7 Quantitative Analysis

Although the ability of qualitative analysis can serve as a powerful tool adequate for many applications, other may require an approach where the presence of an element can be expressed quantitatively. While the qualitative analysis requires simply the presence or absence of a spectral line on a given wavelength, quantitative analysis focuses on the intensity of the specific line or a set of lines. However, quantification capability of the LIBS method is considered as one of the method's limitations. In this case, one of the main advantages of the LIBS method – no need for a sample preparation – turns out to be a great disadvantage for the quantitative analysis as the homogeneity of the sample is limited. For the quantitative analysis to be precise, the variation in the matrix between the sample of unknown concentration and the calibration standard has to be minimal. Effects on analysis results, caused by this variation, are called *matrix effects*.
The differences between compositions of LIBS samples lead to variability in parameters like surface absorption, reflection or thermal conductivity [26]. Combined

with the complex nature of the spatially and time dependent plasma-particle interaction processes, these lead to a strong limitation of quantitative LIBS [15]. Nevertheless, it must be mentioned that, regardless of the mentioned limitations, LIBS sensitivity is usually well under the ppm level for trace elements in solids or liquids [17].

A common way to perform quantitative analysis in LIBS is to construct calibration curves, where the concentration of an element in unknown sample is obtained by comparison with samples with known concentration. A calibration curve, or a curve of growth, expresses the relation between the intensity of a spectral line as a function of element concentration [15]. The curve is determined from a set of standards – samples with known concentration of elements and a matrix similar to the matrix of unknown sample. The ideal shape of a calibration curve is a line plot and the linear fit to the data would pass through the plot origin. However, at the lower and higher concentrations of the sample, nonlinear behaviour of the calibration curve is common. The change in signal for a given increment of change in concentration is called sensitivity and is given by the slope of calibration curve [20]. The sensitivity rises with the steeper slope. To achieve reliable concentrations of desired element, it is recommended to work with linear parts of the calibration curve.

In order to reduce uncertainties occurring due to laser energy fluctuations, non-exact focusing of the laser beam on the sample, or the effect majority element concentration changes in the sample, a method called internal standardization can be used. This approach relates the spectral line intensity of an identified element to another spectral line intensity with known concentration (usually a matrix element) [18]. In general, more accurate results of quantitative analysis are obtained when the internal standardization is used.

Important parameter of a quantitative analysis are the limits of detection (LOD). For a solid sample, the LOD represent the lowest content at which the presence or absence of an element can be determined with a given statistical certainty. In LIBS, the LOD can be expressed as [26]

$$LOD = 3 \cdot \frac{s_B}{S}, \tag{1.8}$$

where s_B is the standard deviation of the signal background and S is the sensitivity of the calibration curve. Alternative ways of defining LOD are stated for example in [15].

2 Remote LIBS Analysis

Because the literature is not consistent in classification of remote LIBS approaches, it would be appropriate to introduce a uniform terminology. The terminology in this text is inspired by the terminology introduced by Laserna and Fortes in their review article [10]. According to how the measurement is performed, remote LIBS can be divided into three basic categories:

- *Portable* LIBS – signal is transferred by an optical fiber. A probe with laser head and focusing optics is close to the sample, carried by an operator. A subsection in this category is *hand-held* LIBS.

- *Remote* LIBS – signal is transferred by an optical fiber. Unlike *portable* LIBS, the probe with focusing optics is not held by an operator, allowing measurements in hard-to-access environments.

- *Stand-off* LIBS – signal is transferred by the surroundings (mostly air), allowing long-distance measurement without the need of accessing the sample.

In following sections, each configuration will be roughly described. Because of the nature of this diploma thesis, more attention will be paid to *stand-off* LIBS configuration.

2.1 Portable LIBS

In *portable* LIBS configuration both the laser pulse and plasma radiation are transferred by an optical fiber. *Portable* LIBS devices are composed of two parts – a hand-held probe and a control unit connected by an optical fiber.
As the probe is held by an operator the main requirement for it is to be as lightweight as possible. For this reason, the probe contains only the laser head and focusing and collecting optics. The sample is approached by the probe from a small distance, allowing the use of focusing optics with small focal length and depth of field (DOF). This is beneficial because a small spot diameter and thus high irradiance in the focal plane of the lens is guaranteed despite the use of lower energy pulses (ones or maximum tens of mJ) [18]. Use of higher energy laser pulses is not possible because of relatively low damage thresholds of optical fibers.
Control unit contains heavier components, such as spectrometer, computer, necessary electronics, battery or a pump. The control unit is commonly located either in a backpack (the operator carries the whole system) or in a suitcase. However, some

interesting ideas of making the device as compact as possible exist – for example in [30] whole LIBS system with all its components was integrated into a vest.

First *portable* LIBS system was developed by Yamamoto et al. [31]. The instrument contained a hand-held probe and a control unit placed in a suitcase. However, the control unit did not contain the battery yet, which reduced the autonomy of the system. The instrument with a total mass of 14.6 kg was designed for analysis of Pb in paints, Be, Pb and Sr in soils and Be and Pb particles in filters [10]. The precision of element determination was in the range from 23 to 47 % and the LOD were in thousands ppm for paints and hundreds ppm in soils. Of course, the results obtained with this device are today overcome by far. Despite this fact, they were comparable to those obtained by XRF and conventional LIBS devices used that time. The design of this device has become a pattern for many future *portable* LIBS instruments that were developed later.

Thanks to the rapid technology advancements in fiber and beam optics, *portable* LIBS devices has become more reliable. Lately, a portable LIBS device was used for analysis of gunshot residues by Fernández et al. in [32]. The results of analysis performed by compact remote LIBS device were compared with results from SEM system equipped with an EDX detector. The study has proven that LIBS is capable of rapid in-situ analysis, being able to detect gunshot residues in samples where number of gunshot particles is ≥ 3 with 100 % reliability.

Common configurations of the probe-control unit arrangements dependent on the application are summarized in Fig. 2.1. Type 1 is suitable for analysis of objects located within the reach of the operator. Type 2 (a and b) is suitable for objects of interest located on the floor or above the operator due to the placement of the laser head allowing longer reach due to the laser head placement. In the Fig. 2.1., common configurations of optics are also shown. While configurations A-C offer only spatially limited spectral information due to the use of both focusing and collecting optics, no collection optics is used in the configuration D. This means that the light is spatially integrated from the plasma volume and the only limitation is the numeric aperture (NA) of the optical fiber. The spatial integration of light means also spatial integration of plasma parameters such as density and temperature. Nevertheless, the use of collection optics is strongly preferred as it results in higher signal coming to the spectrometer [11].

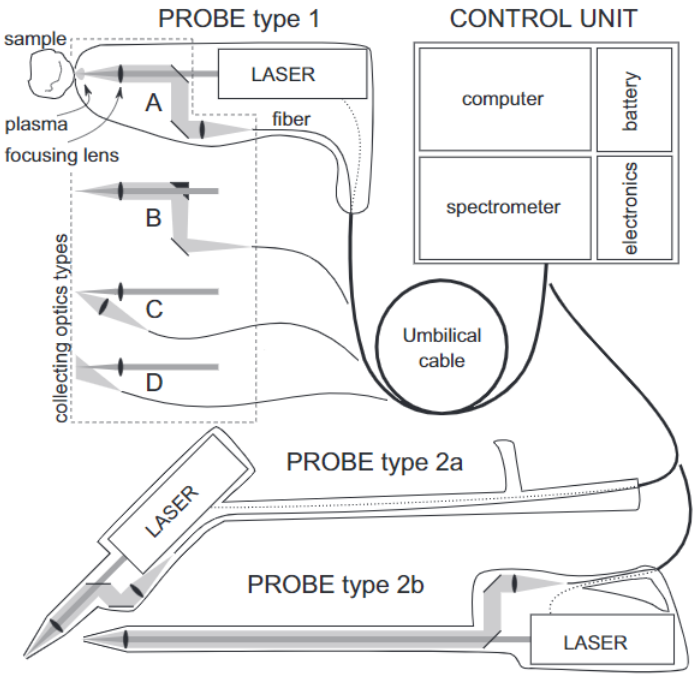

Fig. 2.1: A schematics of a *portable* LIBS device. The Probe unit can be arranged in two types - type 1 being a general concept, type 2a and 2b used for samples located on the floor/above the operator. Four options of light collection are shown, A-C using collecting optics, D - collecting optics is not present and plasma radiation is collected directly by the fiber [11].

2.2 Remote LIBS

Similar to *portable* LIBS, signal is transferred via an optical fiber in *remote* LIBS devices. They also work on the same principle – the device is divided into two parts, one of them being a probe unit and the other being a controller unit. The main difference lies in the way of use of *portable* LIBS and *remote* LIBS devices. While *portable* LIBS devices are used in applications where the sample is reached closely by a person and then analysed, *remote* LIBS instruments are designed for distant measurements. Because of the use of optical fibers, the laser pulse can be led a great distance away from the LIBS apparatus itself. The plasma is collected by a second optical fiber and even the use of the same optical fiber for both focus and light collection is not uncommon. A schematic of common *remote* LIBS optic configurations is shown in Figure 2.2.

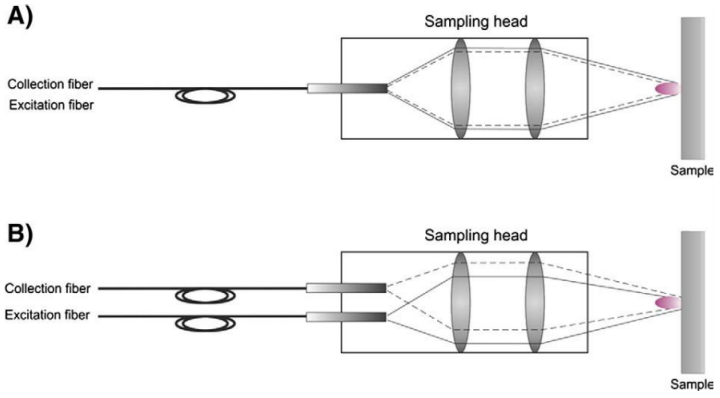

Fig. 2.2: Schematics of two *remote* LIBS configurations. In A), one optical fiber is used both for excitation and for collection of plasma radiation. In B), one fiber is used for excitation and a second one is used for radiation collection [10].

One of the greatest advantages of *remote* LIBS instrumentation is, that the sample can be placed in conditions that are extreme or dangerous for direct access. Unlike *stand-off* LIBS, the sample analysed by a *remote* LIBS device doesn't need to be directly visible, with the only condition being accessible by the probe. As an example, *remote* LIBS device was used in [33] for determining the portion of copper in a steel alloy in two nuclear power stations. With the distance of the sample being 75 m, the device was capable of performing reliable quantitative analysis. The copper concentration LOD was 360 ppm (with 0.0091 % Cu concentration in the alloy). *Remote* LIBS is also successfully being employed in industrial [34, 35] or environmental [36] applications.

2.3 Stand-off LIBS

Although remote LIBS instrumentation including optical fibers is very versatile, it has its limitations. Because the optical fibre is led to a great distance so that the probe could approach the sample closely, its use in toxic or extreme environments is not possible. Moreover, fiber optics is out of the question in those cases when analysis of a larger area on the sample is needed. In these applications an open-path approach named *stand-off* LIBS is needed. In *stand-off* LIBS systems, the laser beam is focused directly onto the sample by focusing lenses, inducing plasma. The radiation of the plasma is then collected by the collection optics. The signal is transmitted by the surrounding atmosphere in both directions. One of possible *stand-off* LIBS configurations is shown in Fig. 2.3.

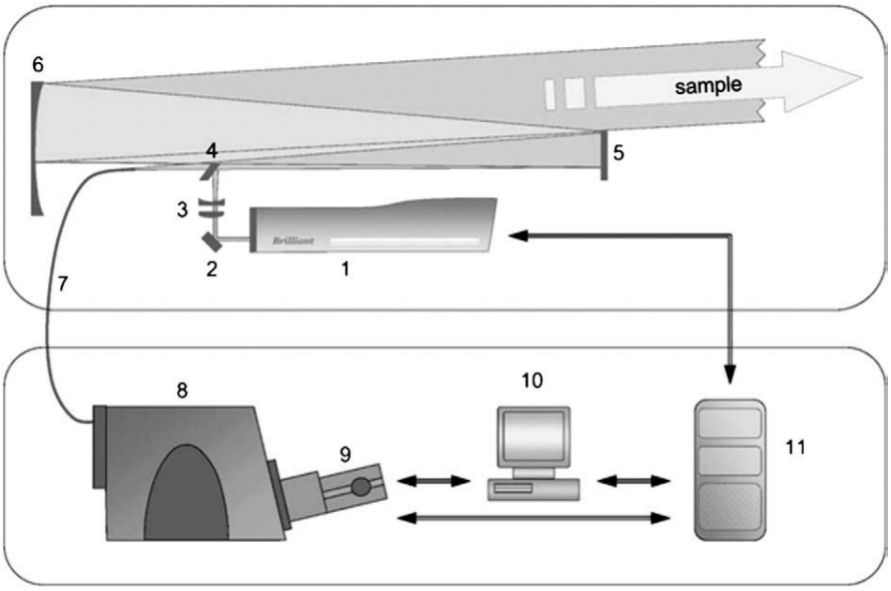

Fig. 2.3: *Stand-off* LIBS instrumentation. Collimated beam from laser (1) is folded by the mirror (2) and broadened by lens system (3). It is then folded by the dichroic mirror (4) and focused by the focusing mirror (5) and the primary mirror (6) to the sample surface. Plasma radiation, coming in the opposite direction, is focused by mirrors 5 and 6 into an optical fiber. The signal then comes onto the slit of spectrometer (8) is recorded on a detector (9) and displayed on the computer (10). 11 is the power supply [10].

As was discussed before, a high irradiance is needed in order to induce plasma on the sample surface (the threshold irradiance for breakdown being around 1 GW·cm^{-2} [37]). In the case of *remote* LIBS instrumentation, this was achieved by focusing of a low-energy laser beam onto the sample with short-focus lenses. On the other hand, *stand-off* LIBS devices need the focusing optics to focus the laser pulse on the sample at a very long distance (typically tens of metres). As a result, the diameter of the spot created on the sample by incident beam is generally bigger. Apart from the aberrations given by the choice of optics, the spot diameter is affected by laser parameters and distance of the sample.

For a given laser pulse power, the irradiance generated on the remote sample is strongly dependent on the minimum spot diameter achieved by the focusing of the laser pulse. If the laser beam profile is close to Gaussian the spot size is governed by the diffraction limit and spherical aberration of the focusing optics [37]. The similarity between a Gaussian and real beam is expressed by the beam quality factor $M^2 \geq 1$, with the value $M^2 = 1$ being true for an ideal Gaussian beam.

In *remote* and *portable* LIBS applications, the focus with small DOF was used

because of the small distance of the probe from the sample. However, in *stand-off* LIBS applications DOF has to be chosen in order to produce greatest irradiance on the sample in a reasonable range. The DOF is defined as twice as long as the Rayleigh length (distance between two positions from the laser waist at which the area beam was doubled [37]:

$$DOF = \frac{8\lambda}{\pi}\left(\frac{r}{D}\right)^2 M^2, \tag{2.1}$$

where r is the distance from the sample and D diameter of the laser beam in the principal plane of focusing lens.

In order to ensure that enough sample material is ablated by the incident laser beam, *stand-off* LIBS systems generally use higher laser energies than *remote* LIBS. In [10], Laserna et al. present that the energy of the laser pulse can reach 1200 mJ for a stand-off LIBS instrument able to perform analysis at the distance up to 120 m.

For analysis in fixed (and shorter) distances, single optical element is used for laser beam focusing. However, in most cases the distance of focus needs to be adjusted. A commonly used arrangement of optics with adjustable focal length is Galilean telescope composed of a convex and a concave lenses, where the focal length is changed with the position of optical elements. The incident laser beam, considered as collimated, is expanded by the concave lens in order to use whole area of the convex lens, which then focuses the beam on the sample.
A more sophisticated solution for laser focusing is combination of refractive and reflective optics (one of these systems can be seen in Fig. 2.3). The use of reflective optics is beneficial because of one simple reason – refractive optics is generally burdened with spherical aberration, leading to bigger spot on the sample. Nevertheless, reflective systems are burdened by off-axis aberrations (such as astigmatism, coma, field curvature or distortion).
To name an example of collecting optics, Galilean telescope and a compact Schmidt-Cassegrain telescope is used for laser beam focusing in ChemCam in MSL (Mars Science Laboratory, more widely known by the name of rover Curiosity). The principle of Cassegrain telescope is simple. Collimated laser beam incident on the primary concave spherical mirror is focused in its focal plane. In front of the focal plane, the secondary convex mirror is placed, focusing the incident beam through a hole in the primary mirror onto the sample surface (schematic of a Cassegrain telescope is shown in Fig. 2.4). The Schmidt-Cassegrain variant employs a Schmidt corrector plate, an aspheric lens used for correction of primary mirror's spherical aberration. By moving the secondary mirror, ChemCam is able to adjust its focal point in the

range of 1.3 – 7 m [38].

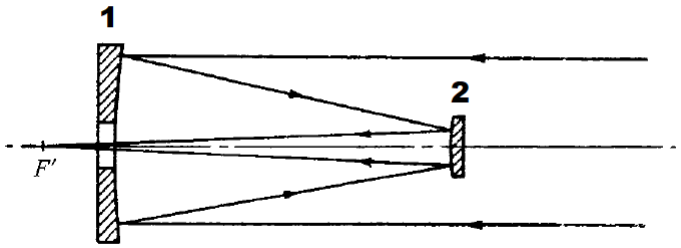

Fig. 2.4: *Stand-off* Schematic of a Cassegrain telescope. 1 is the primary concave spherical mirror, 2 is the secondary convex mirror. Taken from [39] and edited.

While quality of the imagining is the decisive factor for focusing optics, the aim of collecting optics is collecting as much plasma radiation as possible. However, the role of aberration becomes crucial as the aim is not only quantity, but also the need of focusing the plasma radiation into an optical fiber or a spectrometer slit. As was mentioned before, because of spherical aberration of refractive optics, reflective optics is preferred for collection optics. The off-axis aberrations affecting the system are not very significant – because the plasma plume is small (usual diameter moves around 1 mm) and located far from the optical system, it can be considered as a point source. The system is then affected only by diffraction limit and spherical aberration, which is much smaller than in the case of lenses. The limitation of collection optics lies in its dimensions. As the most effective collection of plasma radiation is required, a solution in using bigger collection optics serves itself. Nonetheless, another requirement is that the LIBS device itself is compact, rejecting the idea of big collection optics. Commonly telescopic arrangement is used for plasma radiation collection – in most applications either the Newton telescope or Maksutov-Cassegrain telescope (this arrangement uses a simpler equivalent of Schmidt corrector plate – Maksutov corrector plate which is a convex meniscus lens).

2.3.1 Signal Transfer Limitations

Neuhauser et al. [40] studied the behaviour of fibre optics for long-distance measurements with *remote* LIBS instrumentation. In their work a design of a robust optical fibre was introduced. The fiber was used for remote LIBS analysis, with the authors focusing on plasma beam behaviour inside the fiber. They have shown that the optical fiber should be placed behind the focus of a laser beam so that about 70-80 % of the fiber core is illuminated in order to avoid irreversible damage. They concluded that transmission losses can be neglected for long fiber lengths (tested up to 50 m) at laser wavelength 532 nm. However, they've also proved that absorption losses for UV emission lines (in LIBS in an approximate range of wavelengths $200 - 400$ nm) is a limitation for distances greater than 30 m.

With the growing distance from the sample, the effects of radiation attenuation gain on importance in *stand-off* LIBS devices. The intensity is decreased by the square of distance from the radiation source. Another effect gaining importance with growing distance is the influence of atmosphere itself. Laserna et al. in [41] studied the effects of atmospheric conditions at the maximum distance 120 m. Their TELELIBS device employed a mix of refractive and reflective optics – the expanded laser beam was folded by a dichroic mirror and focused on the sample by a Cassegrain telescope. This telescope served as collection optics as well with the focused plasma radiation coming to the optical fiber located behind the dichroic mirror. They observed the effects of atmospheric conditions turbulences on the performance of TELELIBS device. They proved that for distant objects beam wandering caused by refractive index fluctuations of the surrounding atmosphere occurs. This fact should definitely be taken into account when an analysis of heterogeneous samples is performed. In extreme cases, the laser beam can be focused outside the sample, compromising the reliability of the measurement. Because of that, the sample should be chosen regarding the distance. Nevertheless, their another conclusion was that the effects of signal diminishing due to propagation through atmosphere is very small when compared with the inversed square law of attenuation with growing distance.

3 Braking Tracks Analysis

Braking track analysis provides a powerful data resource needed to correctly determine the cause of car accidents and to prevent their occurrence. In the past, detection and evaluation of braking tracks was performed mostly by one of visual methods (some are listed for example in [6]). Braking tracks generally become clearly visible when the full braking force between the wheel and the road is applied. Determination of exact position where the vehicle started braking is not possible, because it is strongly dependent on the human factor. This prevents measurements via visual methods from being strictly correct.
Modern cars use ABS (anti-lock braking) systems preventing the wheels from locking up, attempting to maintain traction contact with the road. As a result, the braking track itself is harder to be visually detected. This fact, combined with the fact that the determination of braking track starting point is not exact strongly compromises the use of visual methods. For this reason, other analytical methods than visual analysis have to be used. One of possibilities could be the use of chemical analysis.

In [42] the composition of tyre treads was quantified, showing that tyre treads contain heavy metals such as Mn, Fe, Co, Ni, Cu, Zn, Cd or Pb. In this article zinc was used as a means of tyre tread particles quantification. In [6] Prochazka et al. suggested laser-induced obtained in [42], he used Zn as a reference element used to determine the presence of tyre tread residues. His measurements focused on three Zn spectral lines – Zn I 328.23 nm, Zn I 330.25 nm and Zn I 334.5 nm (where I indicates the atomic state transition). In [6, 13] he proved that LIBS can be used as a rapid, inexpensive and reliable method of braking tracks analysis. However, no device focusing on braking tracks analysis as its primary goal has been developed yet. For this reason, research group from Brno University of Technology and CEITEC (Central European Institute of Technology) decided to cooperate on a semi-automated device for braking tracks analysis. Part of this device - the LIBS optomechanical module - is the subject of this diploma thesis.

4 Road-Trace Project

The aim of the diploma thesis is to develop an optomechanical module for chemical analysis of braking tracks by using the LIBS method. This module is a part of Road-Trace instrument, a device composed of two parts: the LIBS module and robotic unit. Intended purpose and function of each part are described in following sections.

4.1 LIBS Module Description

The LIBS module is a compact device that is capable of performing space-resolved analysis. The module is mounted on the robotic unit. The robotic unit is equipped with a motorized two-axes manipulator, allowing the LIBS module to move within the range of 400 x 600 mm (the manipulator is shown in Fig. 4.1).
While most of the LIBS module components have to be mounted on the two-axes manipulator, others can remain stationary. Stationary parts of the module are laser, pulse generator, controlling electronics unit and a portable computer. Laser pulses are led to the mobile part of the LIBS module with system of plane mirrors placed on the robotic unit frame. The mobile part of the module consists of focusing and collecting optics and a compact spectrometer. The total mass of the mobile part of LIBS module should be lower than 2 kg because of two-axes manipulator mechanism limitations. As the main focus of the diploma thesis is design of the mobile optomechanical part of LIBS module, it will be referred to as the LIBS module in further text. The stationary part will be treated separatedly as a part of robotic unit.

During the analysis, the range defined by the manipulator is scanned by the LIBS module. The analysis is performed in discrete points over this range. The distance between these points is variable, however, the minimum possible step is 10 mm. This distance should be adequate in order to cover the area of possible braking track location with sufficient precision. Presence (or absence) of the braking track is determined by presence (or absence) of zinc lines in the emission spectrum. Following three Zn spectral lines will be used for this purpose: Zn I 213.86 nm, Zn I 330.26 nm and Zn I 334.56 nm.

Maximum acceleration of the system during its movement between two points reaches up to $2g$, where $g = 9,81\ \mathrm{m \cdot s^{-2}}$ is the gravitational constant. Because LIBS method is able to perform very rapid analyses, the time between two measurements can be very short. Thus, all parts of the LIBS module including the adjustment of optical elements have to be designed to be robust enough to withstand the rapid

module movement.

The distance between the LIBS module and the road has to be limited due to possible damage. This damage could be either thermal due to high temperature of the road surface, or mechanical when hit by rocks. For this reason, the distance from the road surface should be at least 100 mm.
As the road surface is not perfectly flat, corresponding DOF has to be chosen. To cover road imperfections and still be able to induce plasma on the road surface the DOF should be at least 10 mm. However, the DOF should also be limited by a maximum value in order to prevent breakdown and plasma induction in air. Thus, the depth of field should lie in the range 10 mm $\geq$ DOF $\leq$ 20 mm.

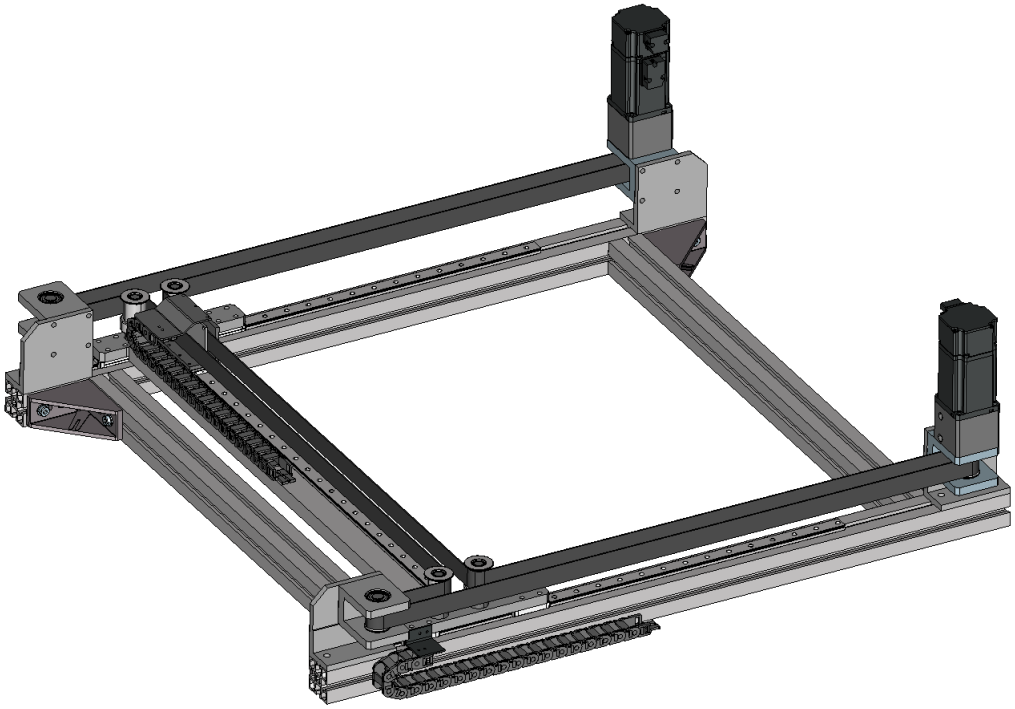

Fig. 4.1: Concept of the two-axes manipulator.

4.2 Robotic Unit Description

The robotic unit carries the LIBS module into a specific location determined for LIBS analysis. The location of the system is then recorded by a control unit based on GPS coordinates input. The control unit also records every movement of the two-axis manipulator, creating a matrix of coordinates. Each set of coordinates is assigned to corresponding measurement output acquired by the LIBS module. This

way, a map of the defined range on the road surface is acquired. The robotic unit is equipped with a camera that serves for visual representation of the measured area.

As was mentioned in Section 4.1, static parts of the LIBS module are placed on the frame of robotic unit. As with every application involving the use of lasers, requirements of user safety have to be met. For this reason, the path leading the laser pulse into the LIBS unit has to be fully optically shielded. Moreover, the analysed area (the range of the two-axes manipulator) is shielded. Whole instrument is covered by a cover sheet from the upper side. Shielding of the area between the frame and the road surface is realised by a retractable cover that is automatically moved down before the start of every measurement. Main parts of the robotic unit are shown in Fig. 4.2.

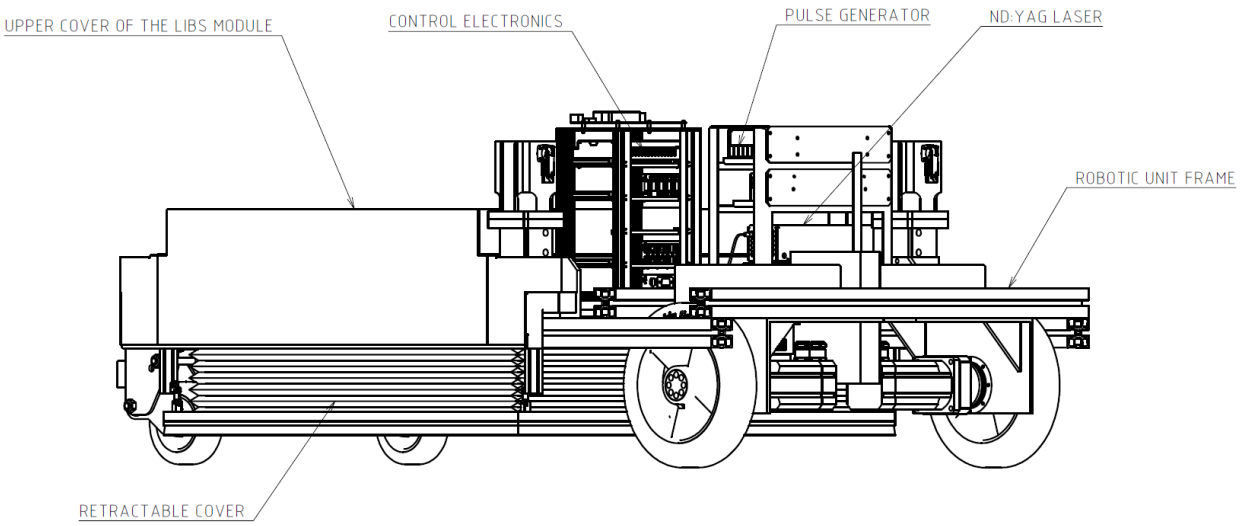

Fig. 4.2: Visualisation of the Road-Trace concept. The positioning of main parts of the robotic unit is visible.

5 Optical Design

Optical components of the LIBS module are divided into two parts - focusing and collecting optics. These two parts are designed separatedly. First, the focusing optics is designed to allow plasma induction on the sample surface. Then the collecting optics, guiding and focusing the plasma radiation into the spectrometer, is designed.

5.1 Focusing Optics

5.1.1 Initial Design

When designing focusing optics for a *stand-off* LIBS device, effects of atmosphere (beam wandering) and distance (inverse square law) should generally be taken into account. However, in the case of the Road-Trace LIBS module, the optics-sample distance is small and these effects will not significantly affect the overall performance of the system. The choice of focusing optics is strongly dependent on parameters of the laser. However, because no specific laser was chosen at the time of initial design of focusing optics, exact parameters of the laser were unknown. To be able to design focusing optics, an estimation of basic laser parameters has to be made.

As was mentioned in section 1.1, solid-state Nd:YAG lasers are chosen for most of LIBS experiments. The primary wavelength of emitted laser radiation is 1064 nm. The pulses can be frequency doubled, thus generating radiation at higher harmonics frequencies with wavelengths 532 nm, 355 nm, 266 nm and 213 nm. Although LIBS experiments frequently use laser wavelengths different from 1064 nm, this choice would not be beneficial for this application. Higher harmonics pulses have the energy lower when compared to the energy of primary wavelength pulse. In most favorable case (wavelength 532 nm), the energy loss would be half of the pulse energy for 1064 nm. For *stand-off* LIBS applications, higher energies of laser pulses are preferred because of the distance between the device and the sample. Last but not least, the generator of higher harmonic frequencies makes the laser head heavier and more expensive.
The aim is to achieve as high energy as possible while keeping the laser compact. The pulse energy 30 mJ was chosen in order to match parameters of commercially available lasers.

First thing that needs to be determined is what focusing lens can be used to match laser parameters and the spatial limitations of the module design. For the focusing to be efficient, the roughness of the sample surface (the road) needs to be

taken into account. Because the road surface is strongly inhomogenous, a proper DOF of the focusing optics has to be chosen in order to compensate inhomogenities. It was decided that the corresponding DOF value would be $DOF = 10$ mm. This value of DOF will be used along the estimated laser parameters for choosing the focusing lens. The first parameter of the lens to be calculated is its focal length f. This parameter is closely related to the DOF - the DOF parameter rises with the growing focal length. For this reason, a focal length corresponding to $DOF = 10$ mm has to be found. Because the laser beam focusing has to lead to plasma induction, another important parameter is its spot size on the sample surface.

Because exact parameters of the laser beam are unknown, let's suppose that the laser beam has ideal Gaussian profile ($M^2 = 1$). The DOF of a Gaussian beam is defined as an axial distance within which the beam radius lies within a factor $\sqrt{2}$ of its minimum value (so called waist radius). The DOF is calculated as twice the Rayleigh distance z_0 [43]:

$$DOF = 2z_0 = \frac{2\pi w'^2}{\lambda}, \tag{5.1}$$

where λ is the laser beam wavelength and w' is the minimum radius in the focus of focusing lens. By placing a lens in the path of the Gaussian beam, it is transformed by the lens (see Fig. 5.1). Let's assume that the lens is placed in the waist of the Gaussian beam. Under typical conditions, the incident laser beam is approximately corresponding to a planar wave [44]. The spot size at the focus of the lens for $z_0 \gg f$(so called *far field*) is approximately given by relation [44]

$$w' \approx \frac{2\lambda f}{\pi D}. \tag{5.2}$$

The only parameter of the Gaussian beam that is known in the image space of the lens is DOF. If we substitute $2z_0 = DOF$ into eq. (5.1) and substitute it to eq. (5.2) an approximate relation for focal length of the focusing lens is obtained:

$$f \approx \sqrt{DOF \cdot \frac{\pi D^2}{8\lambda}}. \tag{5.3}$$

The diameter of laser beam on the lens is unknown - however, let's assume a value in typical range of diameters for selected laser parameters $D = 4$ mm. Thus, the resulting focal length of the focusing lens is $f = 243$ mm.
A singlet with this exact focal length is not commercially available. Thus, to achieve it, two options are possible. The first option is to manufacture a custom lens with the given focal length, the second one is using a suitably chosen system of more lenses. Neither of these options are preferred. The manufacturing of a singlet would be unnecessarily expensive and introducing more optical elements would rise the requirements for precise mounting and adjustment. Instead, a singlet with $f = 250$ mm

could be used.

Because the focus of the chosen singlet is longer than the focal length calculated from the DOF, it is obvious that the DOF value will change. The new $DOF = 10.6$ mm is acceptable. One thing remaining is verification if the irradiance on the sample exceeds irradiance threshold. From eq. (5.2) the spot radius can be determined. For $f = 250$ mm, the spot radius is $w' = 42$ μm, resulting to irradiance 6.6 GW $\cdot$ cm^{-2}, being well above the irradiance threshold (being taken as 0.1 GW $\cdot$ cm^{-2}). However, the real spot diameter will be bigger and thus the irradiance lower. This is caused by aberrations taking effect on a real lens. For this reason, a real spot radius has to be found by simulating a real lens in Zemax software.

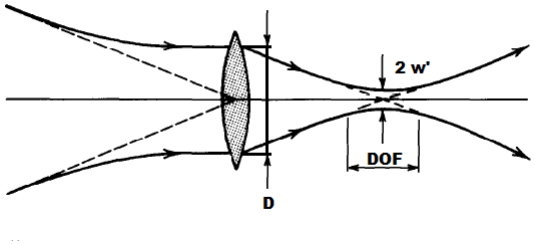

Fig. 5.1: Gaussian beam transformation by a lens. Taken from [43] and edited.

5.1.2 Final Design

Because I decided to use a singlet lens, the lens shape had to be chosen wisely. The spot size is driven by the spherical aberration and the diffraction limit. The spherical aberration rises with the cube of beam diameter on the lens, and can be compensated either by reduction of the aperture or by suitable combination of optical elements. A common practice is to use a convex lens with positive coefficient of spherical aberration and concave lens with negative coefficient of spherical aberration. Another practice lies in the use of aspheric lens. However, aspheric lenses are used for short focal lengths and are not commercially available with the focal length required. The best choice of spherical lens regarding the spherical aberration coefficient is either a plan-convex or a plan-concave lens [45].
Diffraction aberration is caused by the diffraction of light on the borders of the optical element. In an ideal case for real lens focusing, the minimum spot size is determined by Airy disc. The Airy disc is a central circle in the diffraction pattern that corresponds to the first minimum of Bessel function. The region inside Airy

disc contains the majority (83.8 %) of the focused beam energy [39].

A plano-convex singlet lens with 1" (25.4 mm) diameter and $f = 250$ mm was chosen for the design. The material of the lens is UV fused silica (UVFS). This glass is a common choice for LIBS applications because of its high transmissivity in UV wavelength range. Another benefit is its high damage threshold suitable for use with pulsed Nd:YAG lasers and its high transmissivity (over 94%) for the 1064 nm wavelength [46]. By simulating the real lens in Zemax, it was found that the spherical aberration is small and the spot size is diffraction limited (see Fig.). This is caused by relatively high value of focusing lens focal length. With the use of selected lens, the spot radius on the sample surface is 80 µm, resulting in total irradiance on the sample surface 1.9 GW $\cdot$ cm^{-2}. This value is well above the irradiance threshold and the proposed design is suitable for this application.

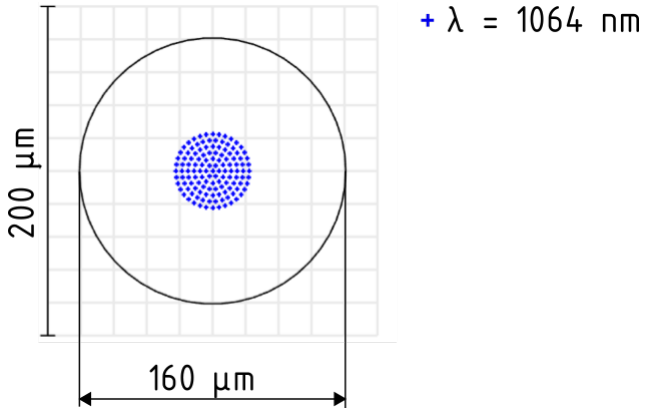

Fig. 5.2: Spot diagram for an axial beam in distance 250 mm from the lens. Although the presence of spherical aberration can be determined from the spherical shape of the spot, the spot size is driven by diffraction (the final spot size is given by the black circle).

5.2 Collecting Optics

The aim of the focusing optics is collecting as much plasma radiation as possible. The diameter of plasma plume, induced on a solid sample surface, is usually around 1 mm. Although the plasma radiates evenly in all directions, only a small portion of its radiation is incident on the collecting optics. The amount of radiation that reaches the optics is given by dimensions of optical elements aperture. This would lead to a tempting solution – using optical elements with bigger aperture. This option is not desirable as the LIBS module has to be as compact and lightweight as possible. Another decisive factor is that increasing aperture size causes increase in aberrations. Thus in order to achieve the best results, quality of optical elements has to be considered. Elements have to be chosen in order to transmit (or reflect, in case of reflective optics) as much radiation incident on them as possible. The choice of elements should be also made with regard to minimisation of aberrations.

Regarding the positioning of collecting optics vs. focusing optics, two possibilities exist – either collinear or off-axis arrangement. In collinear arrangement, the axis of primary collecting optics element is coincident with the focused laser beam axis. In the off-axis arrangement, axes of focusing and collecting optics form a non-zero angle. The off-axis configuration is schematically shown in Fig. 5.3. Collinear configuration examples were shown earlier in the text - see Fig. 2.2 or Fig. 2.3.

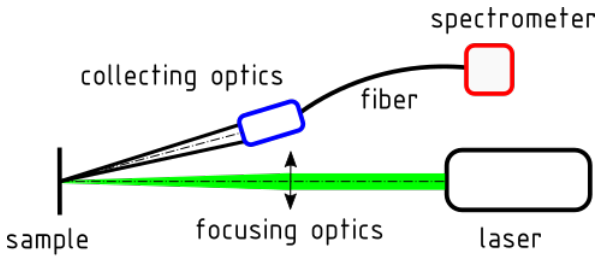

Fig. 5.3: A schematical drawing of off-axis configuration of collecting optics. Plasma radiation is focused by the collecting optics into an optical fiber and is led by the fiber into the spectrometer.

As was mentioned in section 2.3, the use of reflecting over refracting optics is preferred. For shorter distances (up to 2 m [37]), collecting optics can be composed of a lens focusing the plasma radiation into an optical fiber. However, this option will not be further considered, because the use of optical fiber would not have any advantages in this application (the amount of collected light would be lowered for

example by the aberrations of the lens or NA of the fiber).

In the initial design phase, several designs of collecting optics were made. In order to determine the most effective design, proposed options had to be evaluated regarding following parameters:

- Light Gathering Power (LGP) - this parameter determines the percentage of radiation that can be transferred by the optical system to the slit of the spectrometer. Maximum LGP = 1 (or 100 %) is related to the amount of radiation that goes into the entrance aperture of the system under a given solid angle. Other parameters affecting to the LGP are focal length of the system and spot size in its imaging focal plane.

- Mass of optical components - because the mass of the LIBS module is limited, the total mass of each optical design components should be taken into account.

- Price of components - the design should be cost-efficient. This means that primarily commercialy available components should be preferred over custom design.

- Dimension of optical elements - all of designs would share primary optical element dimensions (diameter of the optical element was chosen to be 1"). This way their performance can be compared with the same conditions.

In the initial phase of the design, the choice of position of the collecting optics had to be made. I decided to use collinear positioning of collecting optics. Off-axis configuration could prove as impractical in this application. Because of the sample inhomogenity, the plasma plume could easily get out of collecting optics focus. With collinear collecting optics, the design of the device can be more compact and thus lightweight. Another advantage is that because the optical axes of focusing and collecting optics are coincident, the adjustment of optical elements is much simpler. Nevertheless, together with more comfortable adjustment, the coincidence of optical axes is also a disadvantage. Next to the focusing optics, the laser beam needs to safely pass through the collecting optics element. This can be easily achieved by two ways – by drilling a hole into the element or by using a dichroic filter. Both options are included in following designs.
All designs share the same diameter of primary optical element. This way all the designs can be easily compared by the LGP parameter. The amount of radiation transferred by the spectrometer is limited by its NA. In the case of LIBS module, a

compact spectrometer Ibsen Freedom C-UV is used.

Finally, three options of collecting optics were introduced. Each option was optimised in the Zemax Optic Studio software to achieve best results possible. The results were then compared in terms of their overall performance and viability. Because the distance of the primary optical element is not the same in all cases, a constant solid angle of radiation was taken as a 100 % of LGP. This way, the maximum achievable value should be theoretically the same in all cases.

Spectrometer specification

Because all three desired Zn lines lie in the UV spectrum, a spectrometer with high performance in the UV wavelength range had to be chosen. The spectrometer has to be as compact as possible - this way it can be placed directly in the LIBS module. Placing the spectrometer directly into the LIBS module is required because if the spectrometer was one of stationary parts, an optical fiber would have to be used in order to lead radiation from the LIBS module into the spectrometer. However, a part of signal is lost during the transfer with optical fiber. Another reason why optical fiber is not a viable solution is that since the LIBS module is performing motion along the defined path, placing and retracting of the fiber would be very tricky.
A compact spectrometer Ibsen Freedom C-UV (in Fig. 5.4) was chosen. The dimensions of the spectrometer (61 x 65 x 19 mm) and its low weight (200 g) allow it to be mounted directly as a part of optomechanical module. The spectrometer is suitable for measurements in the UV spectre with wavelength range $190 - 435$ nm. The spectrometer is equipped with a CMOS camera serving as a detector. Entrance slit of the spectrometer has height 750 μm and width 50 μm. Its main limitation lies in the low NA being only 0.11.

Fig. 5.4: Compact spectrometer Ibsen Freedom C-UV [47].

5.2.1 Option no. 1

In the first option, the primary collecting optics element is the same lens that focuses the laser beam onto the sample. Because the plasma plume is located in the focal plane of the lens, it is collimated by the lens. Plasma radiation transmitted through the lens is then incident on a dichroic mirror. This mirror has to be made to transmit the laser wavelength 1064 nm and reflect plasma radiation wavelengths. In ideal case it should have reflectance high enough for the whole range of spectrometer $200 - 450$ nm). Plasma radiation is focused by a refractive optical element into the entrance slit of the spectrometer. An optical scheme of the setup is shown in Fig. 5.5.

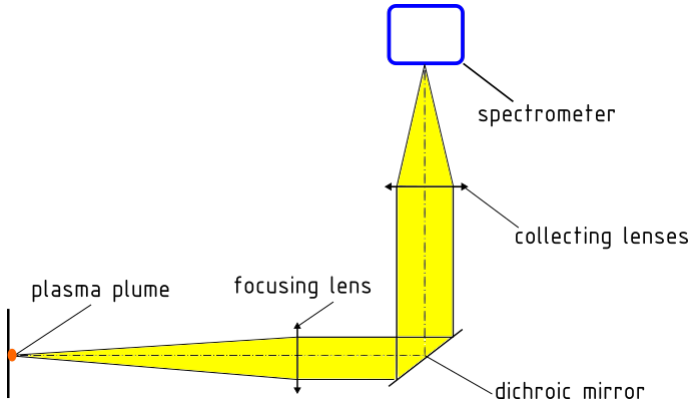

Fig. 5.5: A schematic drawing of the collecting optics. Plasma radiation is displayed in yellow color.

First parameter that needs to be determined while designing the collecting optics is focal length of the system in imaging space. Focal length determines the magnification of an optical system, given by the ratio of focal length in object and imaging

space. Because the aim is to focus as many radiation as possible into the spectrometer slit, a demagnified image is generally desired. Because the focal length in object space is given, total magnification is driven by the focal length in imaging space. Thus, demagnifying the image would also lead to reduction of the module dimensions. However, the amount of radiation (or the solid angle of incoming radiation) that can be accepted by the spectrometer is limited by NA of the spectrometer. If the focal length of the collecting optics would be too short, its performance would be strongly compromised.
A minimum value of focal length, where the optical performance is not compromised by cutting off the incoming radiation, can be found using the Zemax software. In this collecting optics design, the plasma radiation passes through the focusing lens. The plasma radiation is collimated by the collecting lens. Collimated beam is then incident on another optical element - in this case a collecting lens. The question is: What focal length does this optical element has to have in order to not compromise optical performance of the system? A simplified model was created - the collecting optical element was replaced by a paraxial lens. The minimum value of focal length in the imaging space was found to be $f' = 122$ mm (see Fig. 5.6).

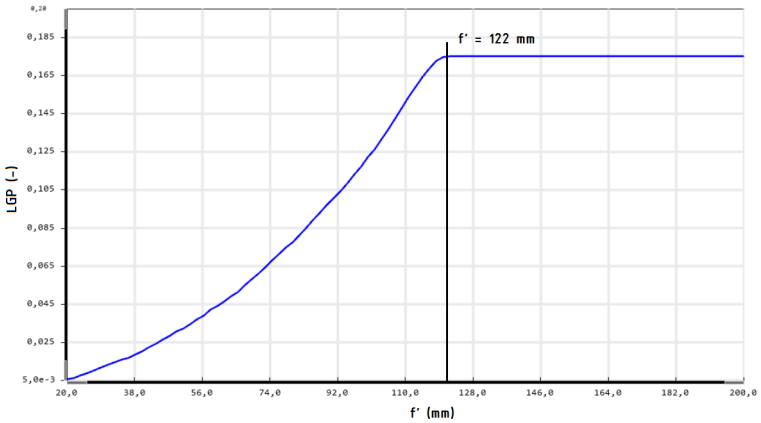

Fig. 5.6: Result of a Zemax computation in order to find an optimal focal length of the collecting optics. As was expected, short focal lengths result in minimum LGP, because the angle of incident radiation is too big. If the focal length in imaging space f' is at least 122 mm, the LGP parameter is not limited by NA of the spectrometer.

Single optical element is not sufficient for effective imaging of the plasma plume because of optical aberrations. Next to the spherical aberration, chromatic aberration also occurs in axial beam image. In classical optics applications, doublets are used in order to reduce chromatic aberration. However, simulations in Zemax

showed that no doublet composed of commercially available lenses is able to achieve sufficient imaging quality. For this reason, a triplet was chosen. The triplet consists of two biconvex lenses and a biconcave lens in the middle. The material of lenses has to be chosen regarding to its transmissivity in the UV range. A combination of CaF_2 biconvex lenses and an UVFS biconcave lens has shown to be the most efficient choice.

Two biconvex lenses with radii of curvature $R = 86.2$ mm and $f = 100$ mm were chosen with an UVFS biconcave lens with $R = 71.9$ mm and $f = -100$ mm between them. Ray tracing through the system is shown in Fig. 5.7. The system focuses the plasma radiation into a spot diameter 553 μm (see Fig. 5.8). The radiation, incoming into the system in a cone with vertex angle 6.9° (equivalent to NA = 0.12) results in a total LGP = (6.4 ± 0.2) %. The low value is caused by many factors. One of them is deffinitely being the size of spot diameter. Although the axial beam can fit the spectrometer slit, a big part of off-axis beams is cut off. Big losses are also caused by absorption (and reflection) of the radiation on surfaces of optical elements. Parameters of the configuration are summarised in Tab. 5.1.

Tab. 5.1: Parameters of the collecting optics in triplet configuration.

LGP (%)	6.4 ± 0.2
Spot diameter (axial object)(μm)	333
Focal length in object space (mm)	250
Focal length in imaging space (mm)	121.8

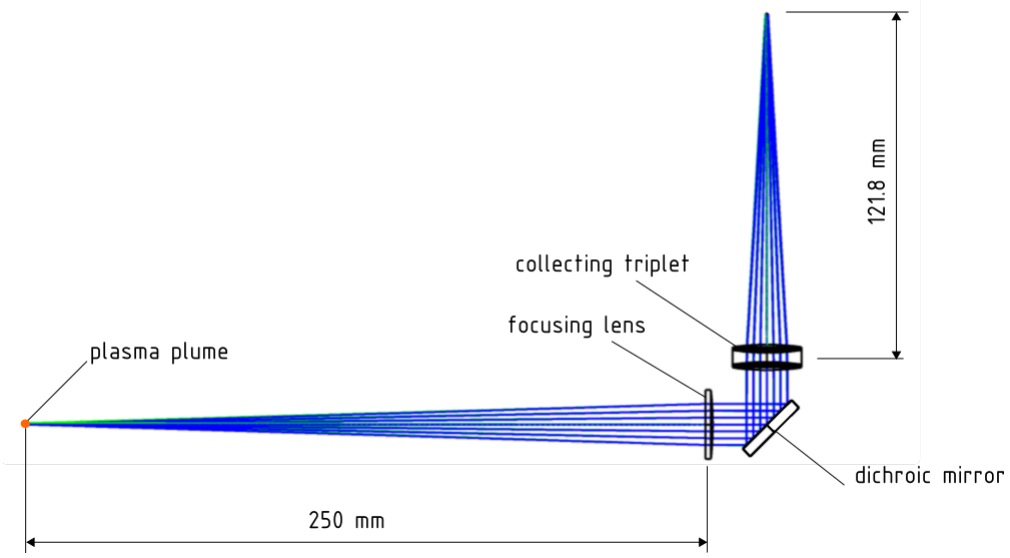

Fig. 5.7: Ray tracing through the system.

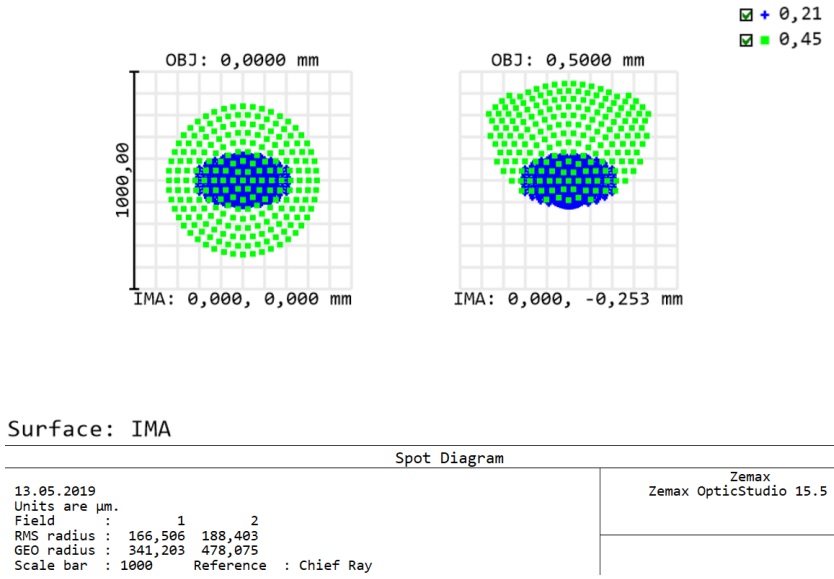

Fig. 5.8: Spot diagram in the focal point of collecting optics in the image space. The diagram on the left shows the projection of an axial beam, on the right is projection of plasma plume boundary. It can be seen that chromatic and spherical aberrations are present. Moreover, coma and astigmatism are visible. In the legend, wavelengths in µm are shown.

5.2.2 Option no. 2

The second design of collecting optics uses the same principle as the previous design. However, instead of triplet, the radiation is focused by an off-axis parabolic mirror. A schematic drawing is shown in Fig. 5.9. The main reason for use of reflective optics is reduction of aberrations. If a collimated beam is incident onto a parabolic mirror surface, it is reflected and focused into its focal point without spherical or chromatic aberrations. A non-collimated beam imaging is burdened by coma. Off-axis mirror is cut off the parent parabola and focuses the incoming collimated beam into the focal point of parent parabola under a given angle.

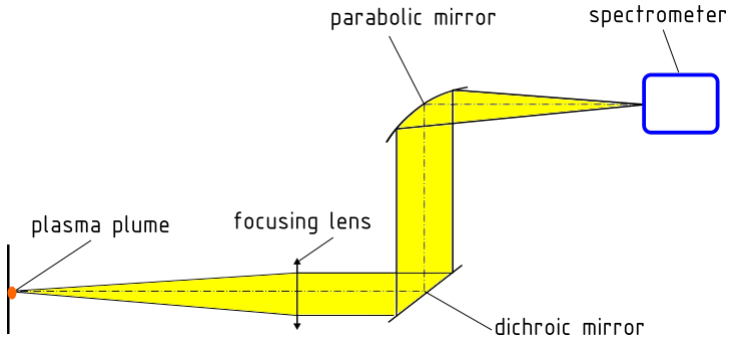

Fig. 5.9: A schematic drawing of the collecting optics. Plasma radiation is displayed in yellow color.

Focal length of the parabolic mirror can be chosen based on the results of simulation shown in Fig. 5.6. From commercially available mirrors a mirror with $f = 127$ mm was chosen. The mirror is made from aluminum and its reflective surface is UV coated. Ray tracing through the system is shown in Fig. 5.10 and the spot diagram is shown in Fig. 5.11. From the spot diagram it can be seen that the spherical aberration and chromatic aberration occur for an axial beam. Aberrations are caused by the focusing lens that collimates the plasma radiation. For the beam coming from the plasma boundary (at distance 0.5 mm from the axis), coma is also visible. From the spot diagram it can be seen that even plasma boundary is projected into the spectrometer slit. As in previous case, the LGP = 1 is taken for plasma radiation incoming to the system with NA = 0.12. The total LGP achieved with this configuration use is LGP = (12.6 ± 0.2) %. Even though the distance of the primary optical element is the same as in option 1, the LGP value is almost twice the value achieved with previous setup. This proves benefits of the off-axis parabolic mirror use. Parameters are summarised in Table 5.2.

Tab. 5.2: Parameters of the collecting optics in off-axis parabolic mirror configuration.

LGP (%)	12.6 ± 0.2
Spot diameter (axial object) (µm)	243
Focal length in object space (mm)	250
Focal length in imaging space (mm)	127

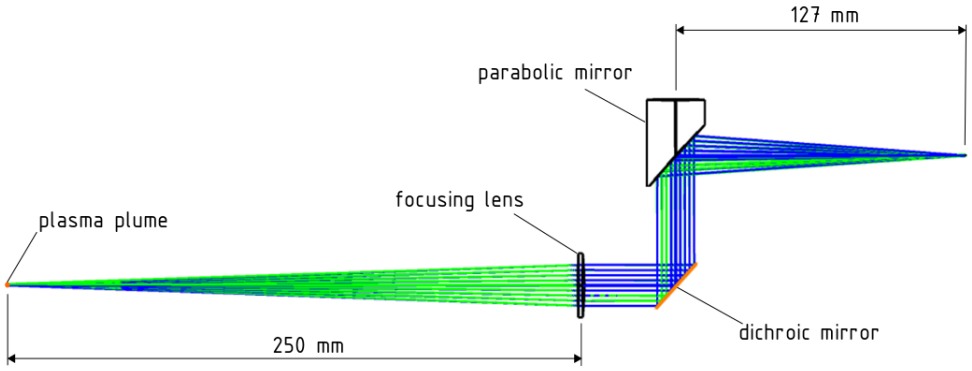

Fig. 5.10: Ray tracing through the system.

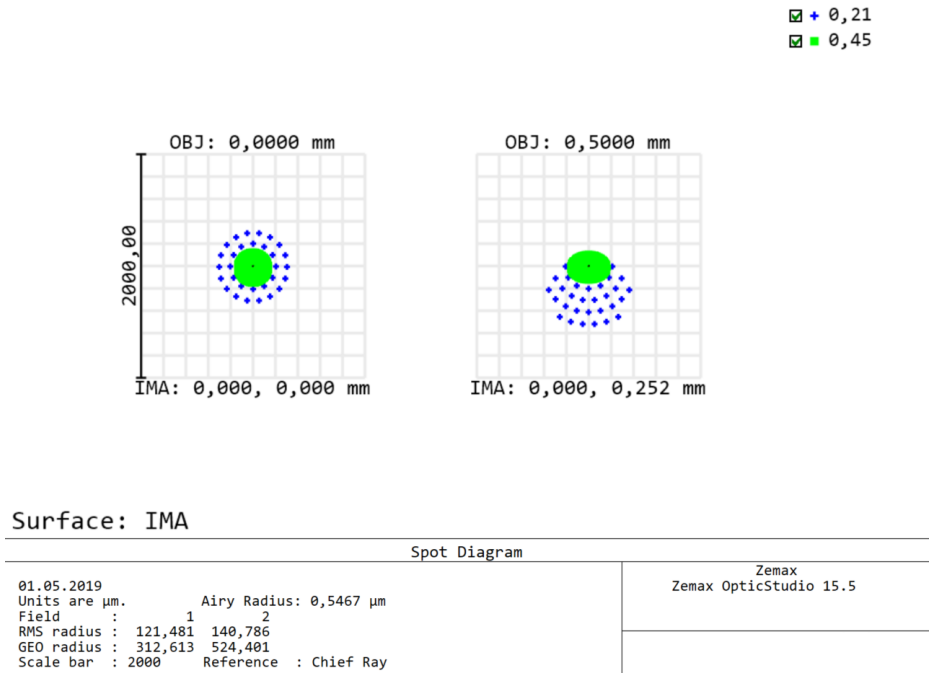

Fig. 5.11: Spot diagram in the focal point of collecting optics in the image space. The diagram on the left shows the projection of an axial beam, on the right is projection of plasma plume boundary. Spherical and chromatic aberrations are visible from the spot diagram. On the right, coma caused by the parabolic mirror can be seen. In the legend, wavelengths in µm are shown.

5.2.3 Option no. 3

As was seen in previous two designs, the fact that the plasma radiation has to come through the focusing lens brings aberrations to the system. In the second design it was apparent that introducing an off-axis parabolic mirror notably improves the system performance. The final design comprises of two axis parabolic mirrors. The schematics is shown in Fig. 5.12. The primary mirror has shorter focal length than the focusing lens. For this reason, it must have a hole drilled through it, so that laser pulse can reach the sample surface. Even though the mirror with hole would have to be manufactured individually, mirror focal lengths are limited by discrete values that are offered by each manufacturer. Although a completely custom off-axis parabolic mirror could be designed, it would be extremely expensive.

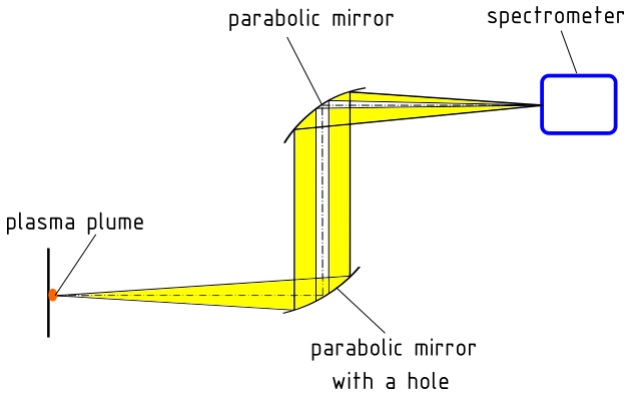

Fig. 5.12: A schematic drawing of the collecting optics. Plasma radiation is displayed in yellow color.

First, a primary mirror was chosen. The shorter distance between the sample and optics, the more plasma radiation can be led through the system. This is not only because plasma intensity diminishes with growing distance, but also because greater solid angle of the radiation is incident on the optical element. Because the smallest distance of the module from the sample is set as 100 mm by the module specifications, I decided to use a mirror with focal length $f = 152.4$ mm. If a mirror with shorter focal length was chosen, it could happen that the total distance of the LIBS module from the road surface.
The second mirror was chosen based on the primary mirror with the same process as in option 1. I modeled a simplified system in Zemax software and optimised it in order to find a minimum focal length of the system so that no radiation would be cut off by NA of the spectrometer. From the graph in Fig. 5.13 it can be seen that for $f = 152.4$ mm the minimum required focal length in imaging space is $f' = 120$ mm.

From commercially available off-axis parabolic mirrors a mirror with focal length 127 mm was chosen.

The system of two off-axis parabolic mirrors was modeled in the Zemax software. Ray tracing through the system is shown in Fig. 5.14. As was mentioned before, the primary optical mirror has to have a hole drilled in its axis so that the laser beam can pass through it. To achieve sufficicient safety, the hole diameter has to be 5 mm. Although the hole diameter seems to be big compared to the total diameter of the mirror (25.4 mm), the loss in LGP was in units of percents. As can be seen in Fig. 5.15, spherical or chromatic aberration does not occur for an axial beam image as was expected. However, in this option no radiation from the plasma boundary is incident on the spectrometer slit. The distance from the optical axis, where the image is starting to be cut off is 0.36 mm (see the spot diagram on the right side of Fig. 5.15). The spot size is diffraction limited for an axial beam and the spot diameter is approximately equal to 4 μm. The total LGP achieved with this configuration is LGP = (39.2 ± 0.2) %. This configuration gives by far the best results. This is caused by closer position to the sample and by the choice of parabolic mirrors. Parameters of the design are summarised in table 5.3.

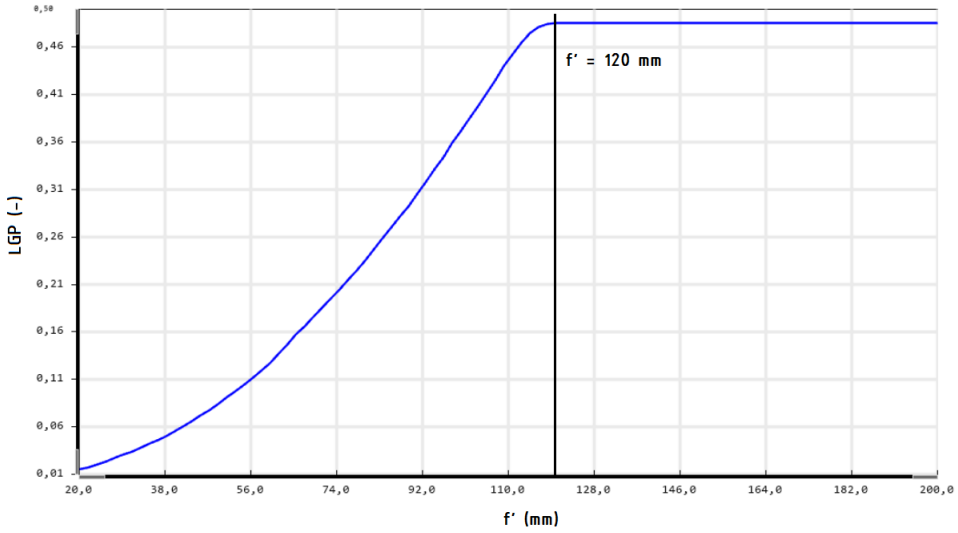

Fig. 5.13: Result of a Zemax computation in order to find an optimal focal length of the collecting optics. As was expected, short focal lengths result in minimum LGP, because the angle of incident radiation is too big. If the focal length in imaging space f' is at least 120 mm, the LGP parameter is not limited by NA of the spectrometer.

Tab. 5.3: Parameters of the collecting optics in two off-axis parabolic mirrors configuration.

LGP (%)	39.2 ± 0.2
Spot diameter (axial object) (μm)	4
Focal length in object space (mm)	152.4
Focal length in imaging space (mm)	127

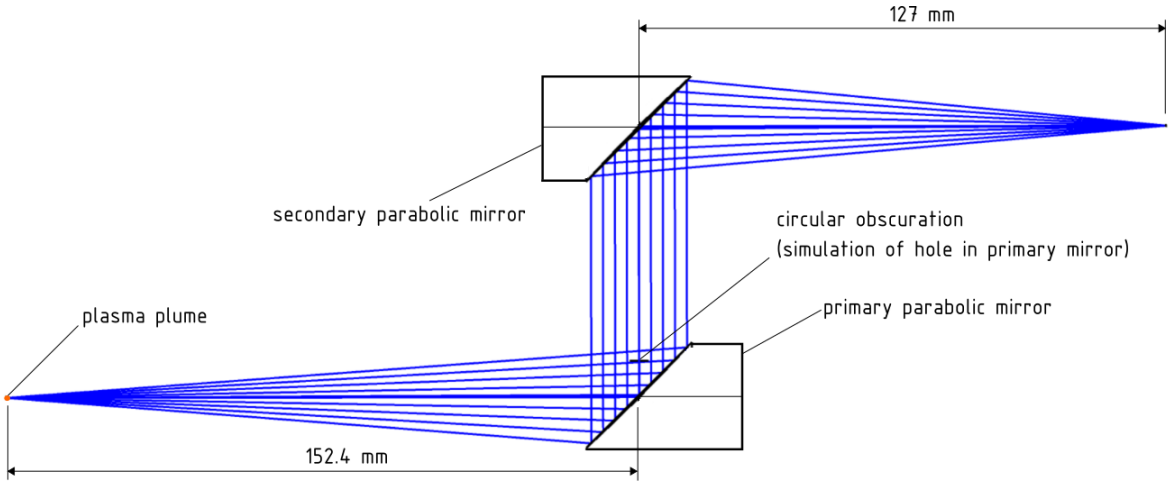

Fig. 5.14: Ray tracing through the system. The hole in the primary parabolic mirror was simulated as a circular obscurration.

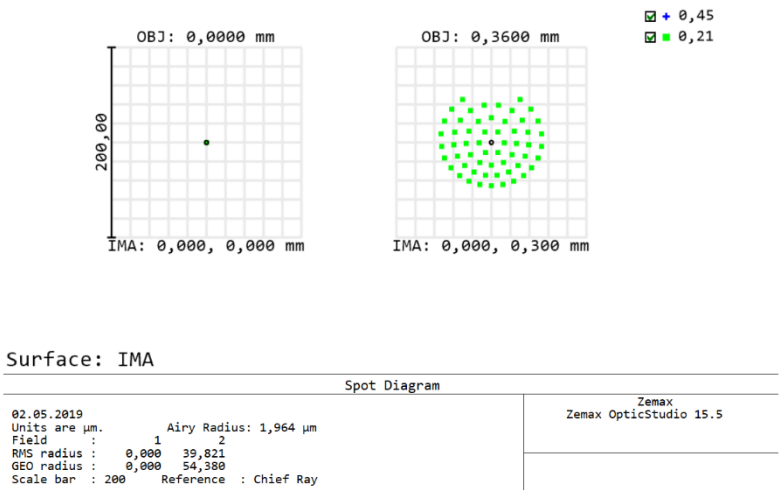

Fig. 5.15: Spot diagram in the focal point of collecting optics in the image space. The diagram on the left shows the projection of an axial beam, on the right is projection of plasma in distance 0.36 mm from the axis, where the image is starting to be cut off. From the image of an off-axis object, it can be seen that no chromatic aberration is present in the system. In the legend, wavelengths in µm are shown.

5.2.4 The Choice of Final Design

Resulting parameters of three optical designs are summarised in table 5.4. Determining parameters are LGP, focal length in the imaging plane, spot size, price and total mass of optical elements (mass and price of focusing lens is included).

Tab. 5.4: Summarisation of optical design parameters.

Design number	1	2	3
LGP (%)	6.4 ± 0.2	12.6 ± 0.2	39.2 ± 0.2
Focal length in object space (mm)	250	250	152.4
Focal length in image space (mm)	121.8	127	127
Spot diameter of axial beam (μm)	333	243	4
Mass of elements (g)	120	100	140
Price of elements (eur)	787.1	551.2	461.3

Regarding the LGP, the design using two parabolic mirrors came out with the best results. This is caused by the quality of the imagining itself. However, the great gap of the LGP in this design versus the other two can be caused the fact that the position of primary optical element is closer to the surface by nearly 100 mm. The focal length of primary parabolic mirror is 152.4 mm, whereas the focal length of focusing lens is 250 mm, and as a result greater percentage of the plasma radiation is incident on the primary optical element. When design no. 1 is compared with design no. 2, where the distance of primary element is the same, it is obvious that the use of parabolic mirror causes better gain. The result is linked with the spot size – the spot size gained with focusing by parabolic mirror is lesser than the size achieved with the triplet. Of course, the best spot size is reached when using only parabolic mirrors – in this case the spot size is theoretically governed by the diffraction limit. Nevertheless, when we compare Figures 5,8, 5.11 and 5.14, it can be seen that while designs no. 1 and no. 2 are able to record the signal from boundaries of plasma plume, the design composed of two parabolic mirror is not able to do so.

Next decisive factor is dimensioning. This is important because of the mechanical design feasibility. The dimensions of the module are determined by focal length in the object and image space. The focal length in the object space is given by the focusing optics in first two designs (250 mm) and by the focal length of primary parabolic mirror in the third design (152.4 mm). The focal length in the image space is different only in the first design, which is caused by the arrangement of lenses into a triplet. However, if the optical elements would be arranged into an assembly, the

third option comes as the best. The distance between the focusing lens and the parabolic mirror would in this case be 97.6 mm, while in previous two cases the dichroic filter can be placed closely to the focusing lens. However, the arrangement of optics in the 3rd design allows the most efficient use of the construction space. The first option is disfavoured the most because it would require additional mirror to bend the plasma radiation by 90 degrees.

The mass of optics does not drastically differ, however, the second design came out as the lightest, while the third design is the heaviest. On the other hand, the third design is the cheapest of all, while the design with triplet is the most expensive.

Based on the result from this section, the third option was chosen for the final design of the LIBS module. It is obvious that its optical performance is the best from all designs presented in this chapter and that it allows the most efficient space usage regarding the mechanical design. However, one more factor needs to be taken into account. As the primary parabolic mirror needs to have a hole drilled through it, it is not possible to buy the mirror as a serial part. Although manufacturers offer mirrors with a hole drilled, dimensions of holes available commercially are not sufficient for this application. For this reason, the mirror would have to be manufactured as a custom part. This would prolong the waiting time and because the design needed to be tested, another solution was chosen. Not one, but two designs would be chosen and tested in laboratory conditions.
Although the second option did not deliver as good results as the third one, all parts are commercially available. Thus, it could be assembled and tested right away. The comparison with the results of third option testing would then reveal if the differences in optical performance were according to the Zemax simulations.

6 Experimental Part

As was was mentioned in section 5.2.4, two configurations of optical design were chosen to be assembled and tested. Testing of both assemblies aims to check following features:

- comparison of adjustment requirements for both assemblies and determining which components need to be mounted on adjustable mounts,
- determination of real depth of field of the collecting optics,
- testing optical designs of both colleting optics configurations in order to see if they are according to results expected from Zemax simulations.

As the main goal of the diploma thesis is to design a device capable of measuring Zn lines in UV spectrum, the system should be able to detect them with high enough intensities. The performance of the collecting optics can be determined based on the intensity of signal acquired by the spectrometer.

6.1 Theoretical Intensity Calculation

Theoretical intensity of an emission line is given by equation (1.6). To determine the intensity, two variables have to be known – transition probability A_{ki} and population density n_k^s of species s. Transition probabilities are listed for example in NIST database [28]. The population density n_k^s is described by the Boltzmann distribution(equation 1.4). If we substitute equation (1.4) into equation (1.6), the intensity can be expressed as

$$I_\lambda^{ki} = A_{ki} n^s \frac{g_k}{U^s(T)} \exp\left(-\frac{E_k}{k_B T}\right). \tag{6.1}$$

Let's assume that electron temperature in LIP is $T = 10000$ K $= 0.867$ eV[1]. For the calculation to be correct, LTE has to be assumed in plasma. The presence of LTE is conditioned by McWirther's criterion (equation 1.2). The number density n^s of species s in LIP can be determined as the minimum electron density for which the McWirther's condition is fulfilled. The partition function $U^s(T)$ for given temperature can be obtained from the NIST database that includes the contribution of all

[1]Instead of kelvins, the electron temperature is often expressed in eV. Temperature 1 K corresponds to $8.671 \cdot 10^{-5}$ eV. This value is given by the ratio of Boltzmann constant to elementary charge.

known energy levels. The partition function was determined as $U^s(0.867\ \text{eV}) = 1.03$. Other variables in equation 6.1 - E_k and g_k - are listed in the NIST database [28] as well.

Theoretical intensities of desired Zn I spectral lines are listed in Table 6.1 along with variables needed for their determination.

Tab. 6.1: Parameters required for theoretical intensity calculation and resulting intensity of Zn spectral lines.

Zn I emission line wavelength λ (nm)	213.86	330.26	334.50
Einstein's coefficient A_{ki} (s^{-1})	$7.14 \cdot 10^8$	$1.20 \cdot 10^8$	$1.70 \cdot 10^8$
Number density of Zn in LIP n^s (cm^{-3})	$3.12 \cdot 10^{16}$	$3.12 \cdot 10^{16}$	$3.12 \cdot 10^{16}$
Statistical weigth g_k (-)	3	5	7
Lower energy level E_i (eV)	0	4.03	4.08
Upper energy level E_k (eV)	5.80	7.78	7.78
Theoretical intensity I_λ^{ki} (counts)	$6.67 \cdot 10^{25}$	$1.87 \cdot 10^{25}$	$3.71 \cdot 10^{25}$

In order to obtain real intensities, radiation losses on optical elements and efficiency of the spectrometer have to be involved. Other parameters that need to be included in the calculation are the LGP parameter (determined in sections 5.2.2 and 5.2.3) and the NA of plasma radiation incident on the collecting optics primary optical element. Intensities that could possibly be gained by testing assemblies are shown in Table 6.2. However, it has to be noted that this calculation has rather informative characteristics. Intensities gained during the experiment are not expected to match the calculated values. However, absolute values should be proportional.

Tab. 6.2: Comparison between intensities of spectral lines calculated by equation (6.1) and between intensities involving losses. Configuration 1 is collecting optics design using a focusing lens, dichroic mirror and an off-axis parabolic mirror. Configuration 2 is the collecting optics design using two off-axis parabolic mirrors.

Wavelength (nm)	213.86	330.26	334.50
Theoretical intensity I_λ^{ki} (counts)	$4.72 \cdot 10^{25}$	$3.59 \cdot 10^{24}$	$6.85 \cdot 10^{24}$
Expected intensity for conf. 1 (counts)	$4.23 \cdot 10^{15}$	$4.51 \cdot 10^{15}$	$1.09 \cdot 10^{16}$
Expected intensity for conf. 2 (counts)	$2.14 \cdot 10^{17}$	$8.42 \cdot 10^{16}$	$1.67 \cdot 10^{17}$

From table 6.1 it can be seen that from all Zn spectral lines in the measured wavelength range, the Zn I 213.86 nm line should be the dominant one. The intensity of this line is twice the intensity of the Zn I 334.50 nm line, which is the second highest.

From results shown in Table 6.2, a loss of signal due optical elements is apparent. Losses are more significant for configuration using the focusing lens, dichroic mirror and parabolic mirror for plasma radiation collection. This corresponds to results of Zemax simulations. With this configuration, a great loss of plasma radiation occurs for Zn line with wavelength 213.86 nm. Highest intensity should thus be observed for Zn I 334.50 nm line. This result is caused by low reflectance of the used dichroic mirror for 200-300 nm wavelength range. No commercially available dichroic mirror is able to achieve reflectances greater than 90 % for all three desired wavelengths. Based on my query in multiple companies offering production of custom dichroic filters, designing an ideal filter for this application would cost approximately 6 000 dollars. For comparison - the price of the dichroic mirror that was finally bought was 250 $. For this reason a compromise was made and a commercially available mirror was bought at the cost of losing a notable part of signal from the 213.86 nm emisssion line.
The results obtained in table 6.2 should be proportional with the experimental results gained with collecting optics configuration using two parabolic mirrors. With the fact that the Zn I 213.86 nm line should have significantly higher intensity than the other two, this should lead to better overal performance of this setup.

6.2 Testing Assemblies - Initial Tests

6.2.1 Configuration with Dichroic Mirror

The first testing assembly is based on optical design described in section 5.2.2. The assembly is shown in Figure 6.1.

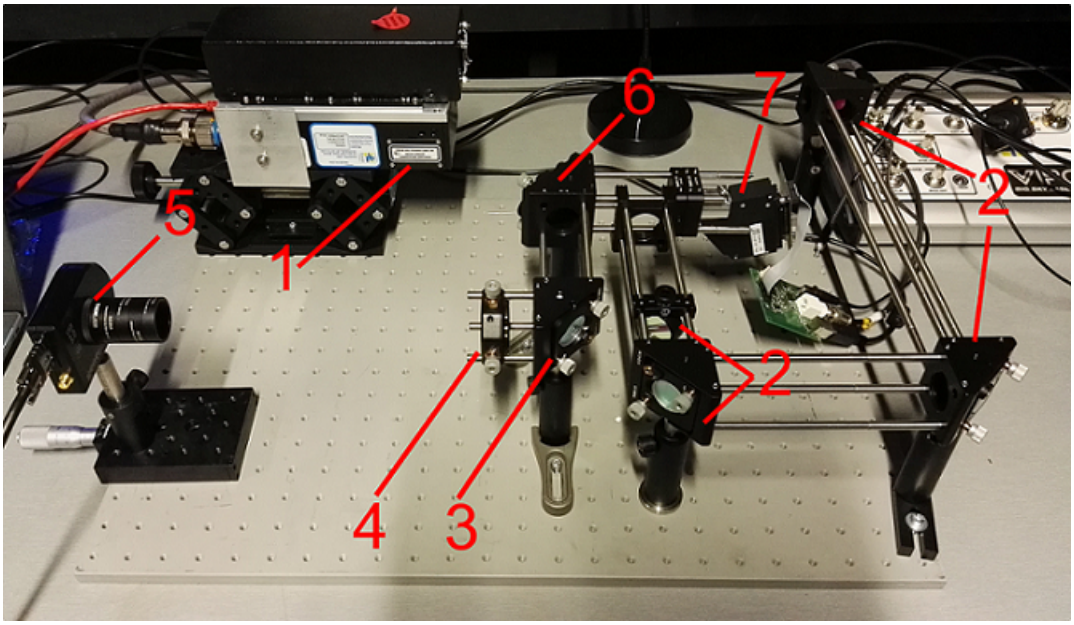

Fig. 6.1: Testing assembly in configuration with dichroic mirror. 1 - Nd:YAG pulsed laser, 2 - plane mirror, 3 - dichroic mirror, 4 - focusing lens, 5 - sample, 6 - off-axis parabolic mirror, 7 - Ibsen spectrometer.

The testing assembly is fully composed by commercial parts. A Nd:YAG pulsed laser Quantel Viron (1) generates pulses with $\lambda = 1064$ nm and frequency 20 Hz. The laser is mounted on a laboratory jack, allowing to adjust vertical position of the laser beam. The path of the pulse is folded by a set of four plane mirrors (2). First three mirrors are placed in kinematic mounts with $\pm 4°$ pitch and yaw adjustment. In the final design, these mirrors would be placed on the robotic unit frame outside the LIBS module. The last plane mirror is mounted differently to fit it better to the cage construction. The mirror can be rotated by 360° and the adjustment is not as precise as for the mount of first three mirrors. Thus, fine adjustment is made before the pulse reaches the fourth mirror. The dichroic mirror (4) is mounted on the same kinematic mount as plane mirrors, allowing the adjustment of reflected beam by $\pm 4°$. The focusing lens is mounted on an XY translation mount. Its distance from the sample is not adjusted. Instead, the sample (5) is mounted on a stage allowing it to

move in 25 mm range (in this case the beam profiling camera is placed in the sample position). The off-axis parabolic mirror (6) is mounted in kinematic mount for off-axis parabolic mirrors. This mount allows pitch and yaw adjustment ±4°. The possibility of off-axis mirror adjustment is crucial because the spectrometer (7) can be only moved along the cage rods. Mounting the spectrometer in a kinematic mount was not preferred regarding feasibility of final mechanical design of the module.

Test of Optical Performance

The test of optical performance was conducted by measuring the spectrum of a mercury-argon calibration lamp. The signal from the lamp was led by an optical fiber to the sample position. The spectrum obtained by this configuration is shown in Fig. 6.2. Three lines of Hg were chosen close to the wavelength range of desired Zn spectral lines and their relative intensities were measured. Results are shown in Table 6.3.

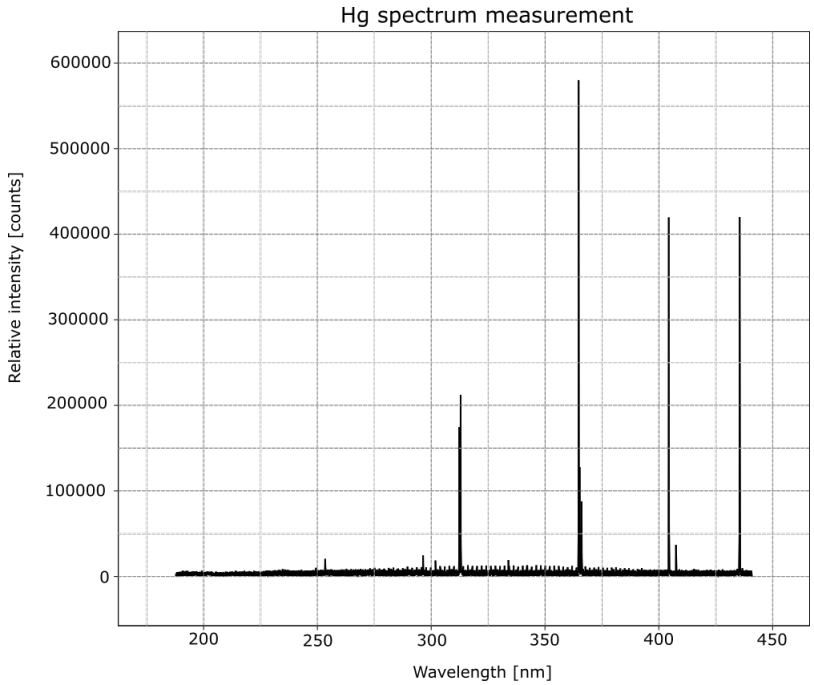

Fig. 6.2: Hg spectrum measured with a Hg-Ar calibration lamp.

Tab. 6.3: Measured intensities of chosen Hg spectral lines.

Wavelength (nm)	Relative intensity (counts)
253.65	$1.97 \cdot 10^4$
313.16	$2.05 \cdot 10^5$
365.01	$5.77 \cdot 10^5$

6.2.2 Configuration with Two Off-Axis Parabolic Mirrors

The focusing part of the testing assembly remains the same as in previous configuration. I've left the dichroic mirror in the assembly, because it doesn't have any impact on plasma induction doesn't collide with the plasma radiation collection. Two off-axis parabolic mirrors are used for plasma radiation collection. Both the primary parabolic mirro (5 in Fig. 6.3) and the secondary parabolic mirror (6) were mounted in kinematic mounts used in previous configuration. This configuration could not be assembled properly. The primary parabolic mirror should have a hole drilled through it in order to allow collinear laser focusing and plasma radiation collection. Nevertheless, because of problems with suppliers, the mirror was not manufactured at the time of submitting the diploma thesis. A substitute mirror with the same focal length was used instead and an off-axis configuration was assembled. The assembly is shown in Fig. 6.3. This fact caused severe limitations in the whole experimental part of the thesis. However, some of the essential tests could still be performed.

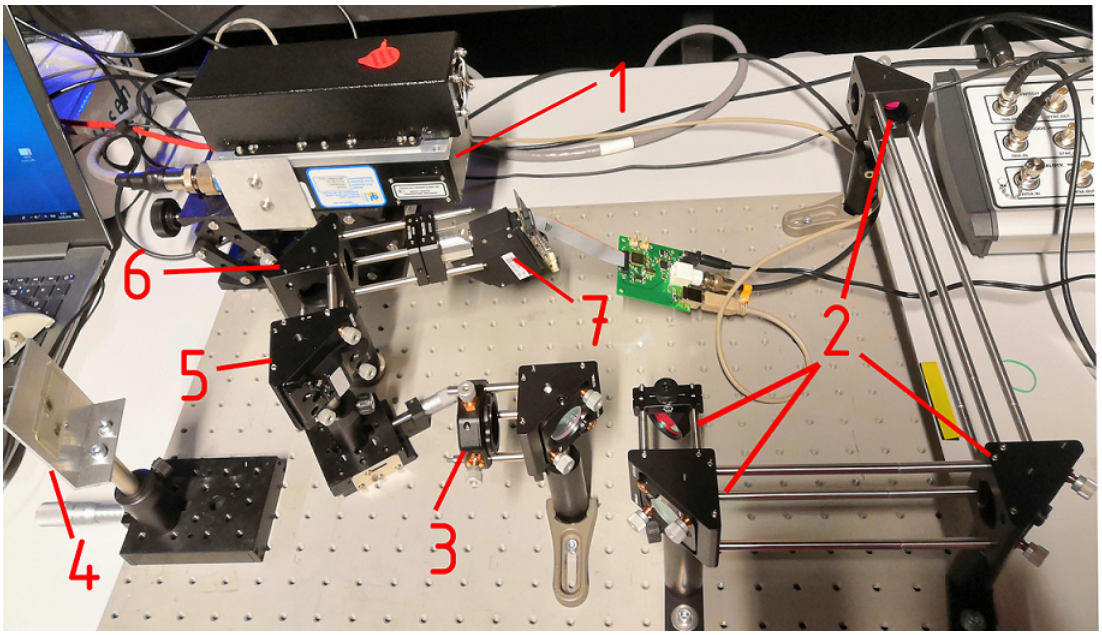

Fig. 6.3: Testing assembly in configuration with two off-axis parabolic mirrors. 1 - Nd:YAG pulsed laser, 2 - plane mirror, 3 - focusing lens, 4 - sample, 5 - primary off-axis parabolic mirror, 6 - secondary off-axis parabolic mirror, 7 - Ibsen spectrometer.

Test of Optical Performance

The test was conducted the same way as in the case of configuration with a dichroic mirror. The Hg spectrum of the mercury-argon calibration lamp was obtained. The spectra obtained by measuring in each configuration are compared in Fig. 6.4. Intensities of selected Hg lines obtained for the second configuration were measured. Resulting intensities of spectral lines measured with this configuration are noted in Table 6.4. When compared with results of the same test in dichroic mirror configuration (Table 6.3), it is obvious that intensity of the 253.65 nm spectral line is two orders higher in this configuration and is domminant for the whole spectrum.

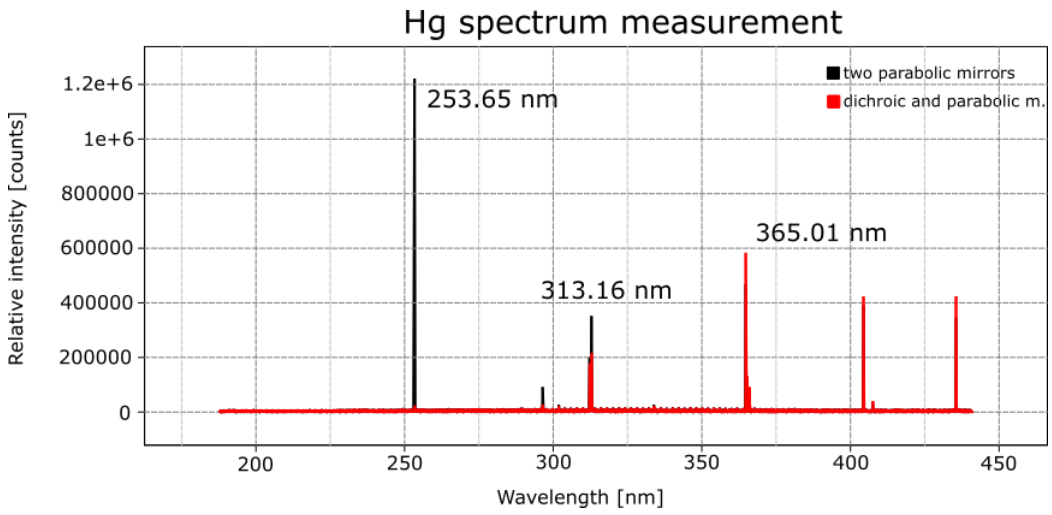

Fig. 6.4: Hg spectrum measured with a Hg-Ar calibration lamp. Spectrum measured in the configuration with two parabolic mirrors is drawn by black line, spectrum measured in the previous configuration with dichroic mirror is drawn red.

Tab. 6.4: Measured intensities of chosen Hg spectral lines.

Wavelength (nm)	Relative intensity (counts)
253.65	$1.22 \cdot 10^6$
313.16	$3.72 \cdot 10^5$
365.01	$5.02 \cdot 10^5$

6.3 Testing Assemblies -Solid Sample Measurements

The previous section described the testing assemblies themselves and their optical performance with respect to expected results. The point was to prove or disprove whether the real assemblies performances are according to expected theoretical results. However, the test was performed on a calibration lamp with a known emission spectrum. For the tests to better simulate real conditions, measurements on real samples should be performed. This includes proper adjustment of the focusing and collecting optics, measurement of DOF and finally obtaining emission spectra of real tyre samples.

6.3.1 Configuration with Dichroic Mirror

Assembly Adjustment

The aim of the assembly adjustment is to unify the point into which the focusing optics is focusing the laser beam with a point from which the plasma radiation is collected.
First, an aluminum sheet was used as a sample. The plasma was induced with the Nd:YAG laser. An aiming green laser was used instead of spectrometer in order to replicate the path of plasma radiation. However, it turned out that the plasma induced on the sheet is so strong that it is impossible to precisely adjust focal points of focusing and collecting optics into one point. For this reason, a different approach using the beam profiling camera was chosen. The precise position of focusing and collecting optics focal points can be found by unifying positions of focal points on the camera chip. First, the focus of focusing optics was found and its position noted. Then, the position of collecting optics focal point was adjusted in order to match the position of focusing optics focal point. From the comparison of positions obtained in Fig. 6.5 and 6.6 it can be seen that although the positions are very close, they are not exactly the same. This is caused by the limitation in optical mounts adjustment precission. However the precision in tenths of mm is commonly accepted as sufficient.

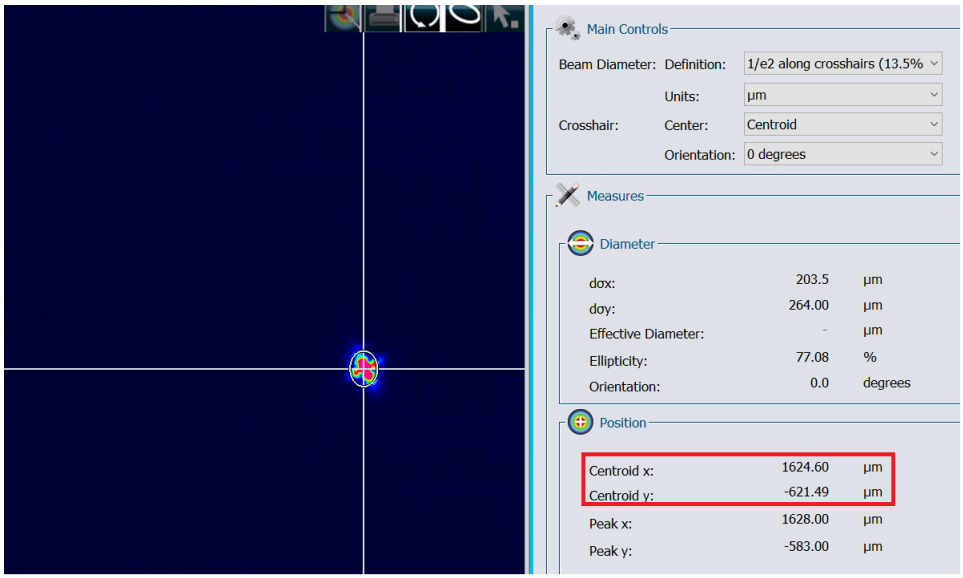

Fig. 6.5: Position of the spot created by focusing the Nd:YAG laser pulse on the beam profiling camera detector in configuration with dichroic mirror. The spot coordinates are marked with the red rectangle.

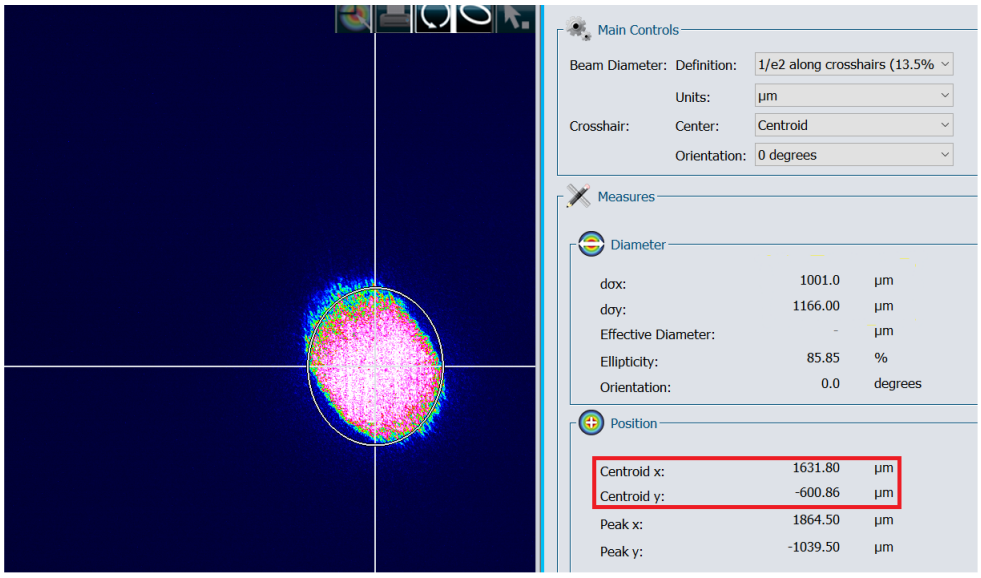

Fig. 6.6: Position of the spot created by focusing the aiming laser on the beam profiling camera detector in configuration with dichroic mirror. The spot coordinates are marked with the red rectangle.

Depth of Field Determination

The DOF of the optical setup was determined by measurements performed on the SUS-1 R reference sample. This sample was used because its spectrum is rich on spectral lines (this is caused by the presence of Fe in the sample) in the wavelength range of the spectrometer. Thus, from the spectrum of the SUS-1 R reference sample the DOF can be determined through the whole wavelength range.
The sample was mounted on a stage at a rough distance 250 mm from the focusing lens. Spectra were obtained from the whole range of the stage, with a default position in the middle of the stage feed. The distance between spectra measurements were 1 mm and 50 measurements were performed in one position. The laser frequency was set to 2 Hz and gate width was 1 µs. From the spectra obtained by this measurement, five intervals around peaks roughly covering the whole spectra were selected (see Fig. 6.7). Peaks enclosed by the intervals were then used as a reference for the DOF determination. The results are shown in Fig. A1-A5 in appendix A.

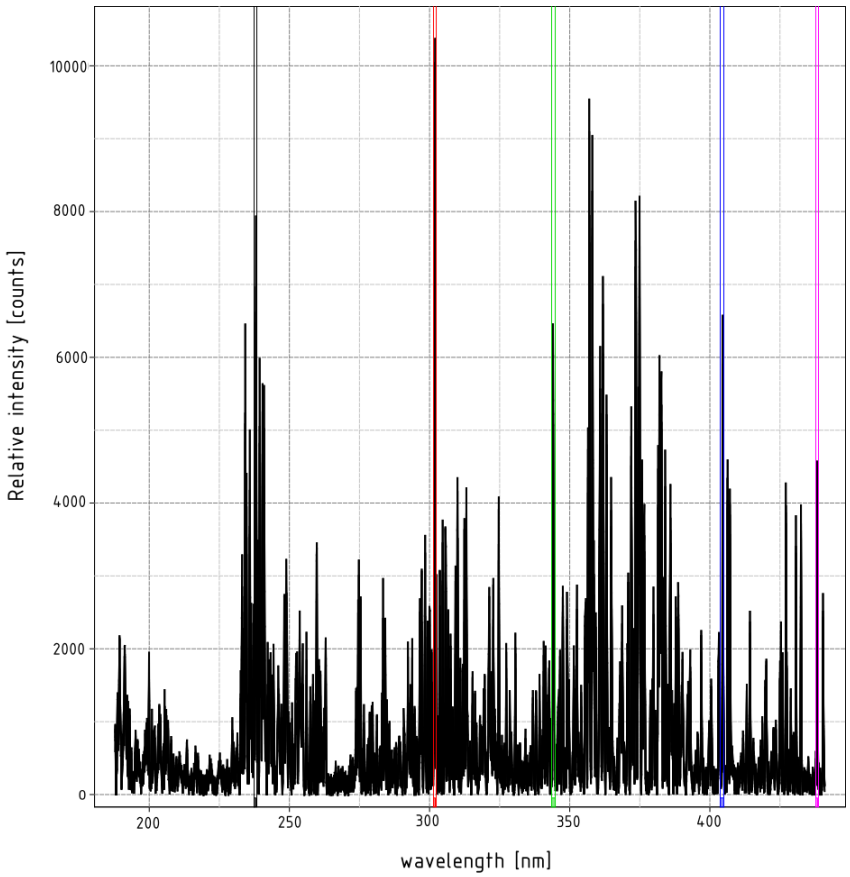

Fig. 6.7: Spectrum of the SUS-1 R sample. Five spectral lines in the spectral range were chosen.

From results of the DOF measurements in Fig. A1-A5, we can see that DOF could not be determined for the Fe II line at 238.09 nm. This is caused by limited performance of the optical setup in middle UV region (approximately 200 - 300 nm). However, all other measured regions show the same results - a region occurs around the position with local minimum where the intensity is the highest. This region can be determined as the DOF. The occurance of the local minimum in the point where we would expect a maximum can be explained by two reasons. First one may be measurement error in this position. However, it is more likely that this point is exactly the focal point of the focusing lens. As the laser pulse is focused into the tighest spot (waist of the Gaussian beam), the effective volume of ablated plasma is smaller than when the laser pulse is slightly defocused. This can paradoxically lead to obtaining worse results than when the laser pulse is defocused. DOF is not the same for all measured wavelength regions. DOF, determined for each range around a certain emission line is shown in Table 6.5. The DOF measured is lower for the 302.02 nm emission line, which is caused by lower reflectance of the dichroic mirror for this specific wavelength. The average DOF (excluding the first spectral line) was determined as DOF = (15.5 ± 0.5) mm.

Tab. 6.5: Determination of DOF for five chosen spectral lines.

Emission line	DOF (mm)
Fe II 238.09 nm	-
Fe I 302.02 nm	14
Fe I 344.01 nm	16
Fe I 404.55 nm	16
Fe I 438.21 nm	16

Limits of Detection Determination

LOD is an important parameter showing the sensitivity of the system. In order to determine LODs, the calibration curve has to be built. Five tyre samples were used for the analysis. First, content c_{Zn} of Zn in each sample was determined using XPS analysis. The spectra obtained by XPS were measured using the Kratos Axis Supra spectrometer [48]. Zinc contents measured by XPS in tyre samples are shown in Table 6.6.

Samples were measured on the testing assembly with gate delay set to 1 µs and laser frequency 2 Hz. Only 25 measurements for each sample were taken, because most of samples tended to be quickly destroyed by the laser pulses. The calibration curve is shown in Fig. 6.8.

Tab. 6.6: Contents of Zn in five tyre samples measured by XPS analysis.

Sample	Zn content (%)
Clio	0.99
Octavia	1.00
RX-8	1.06
Formula tyre bulk	1.72
Unknown tyre	2.09

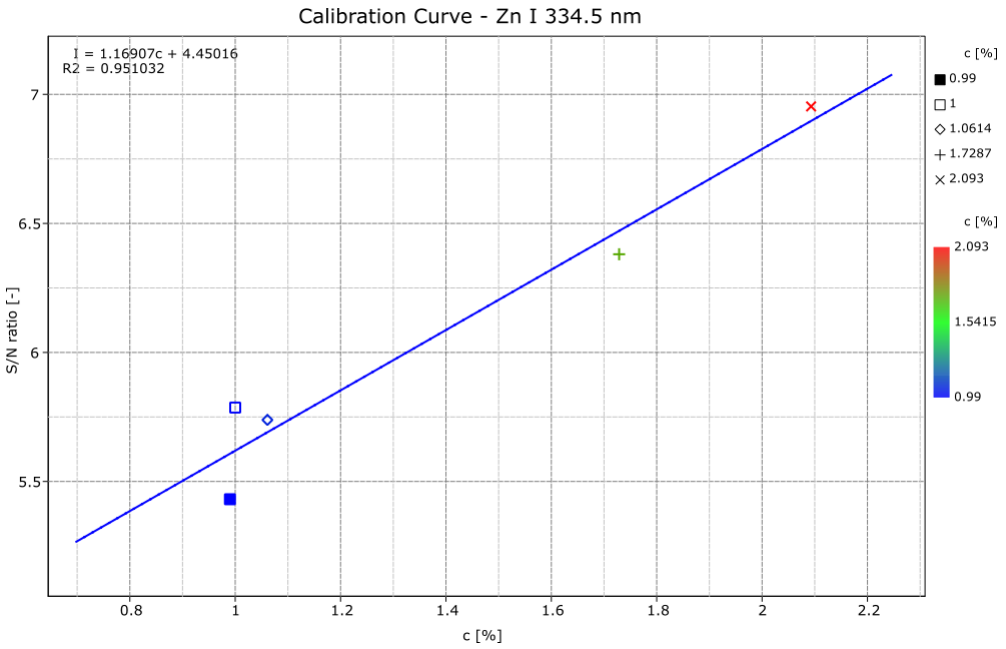

Fig. 6.8: Calibration curve plotted for the Zn I 334.5 nm spectral line. Concentration of the samples is plotted on the x axis, the signal to noise ratio is on the y axis.

From the slope of the calibration curve, LOD for Zn can be calculated using equation 1.8 (section 1.7). The resulting LOD for zinc are LOD = (0.75 ± 0.05) %.

6.3.2 Configuration with Two Off-Axis Parabolic Mirrors

Assembly Adjustment

The assembly adjustment was performed with the use of beam profiling camera. First, the laser pulse was focused into the beam profiling camera (Fig. 6.9). Then, the aiming laser was placed instead of spectrometer and was focused in the position of laser focus. In the previous case, an exact position of the aiming laser focus could by found by moving the camera along the stage range. However, because the focusing and collecting optics were not placed collinearly, this was not possible. For this reason, several iterations had to be made in order to match the focal point of the aiming laser and the Nd:YAG laser. Finally, a focal point of both the collecting and focusing optics was found (Fig. 6.10). However, this has later proven to be worthless. With the testing of real tyre samples, the point at where the plasma was induced changed with each measurement because of inhomogenity of sample thicknesses. The sample position had to be adjusted. This fact caused no problem in previous configuration, but shown to be a great limitation in the configuration with two off-axis parabolic mirrors.

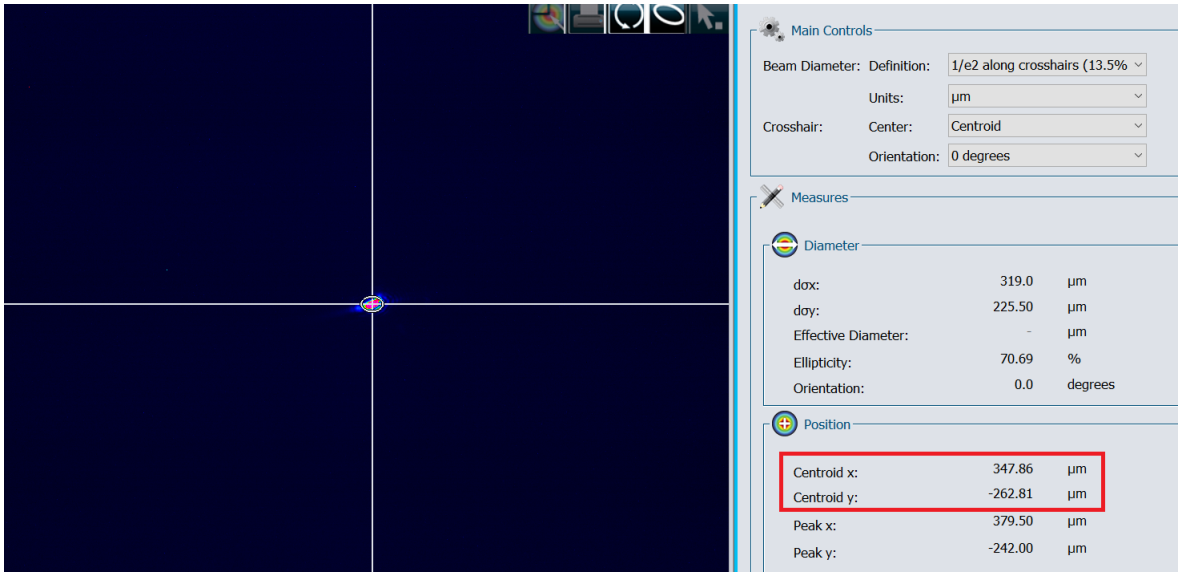

Fig. 6.9: Position of the spot created by focusing the Nd:YAG laser pulse on the beam profiling camera detector in configuration with two off-axis parabolic mirrors. The spot coordinates are marked with the red rectangle.

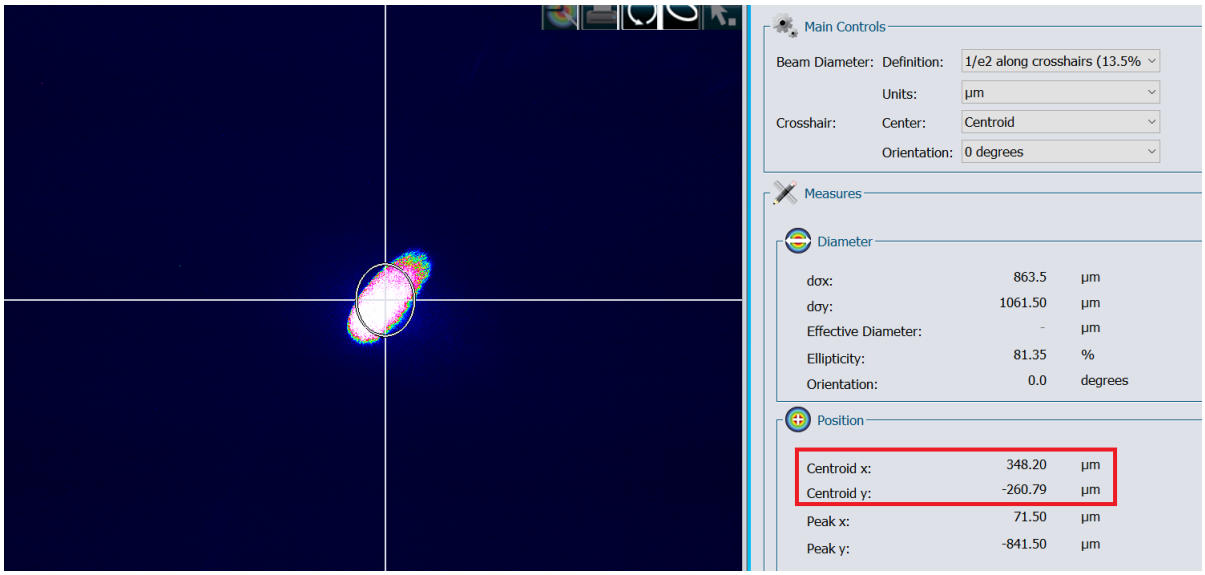

Fig. 6.10: Position of the spot created by focusing the aiming laser on the beam profiling camera detector in configuration with two off-axis parabolic mirrors. The spot coordinates are marked with the red rectangle.

Depth of Field Determination

As a result from the off-axis arrangement of collecting and focusing optics, moving the sample would result in breaking the adjustment of the optics. All atempts made to measure the DOF were unfortunately unsuccessful and thus the DOF could not be determined.

Limits of Detection Determination

Another impact of the off-axis configuration was discovered when I attempted to measure spectra of different tyre samples. Because the samples were taken from car tyres, their dimensions were slightly different from one sample to another. The optical setup had to be re-adjusted prior to every measurement. However, precise adjustment of the focusing and collecting optics focal points could not be done. Using the beam camera would be meaningless, because the position of camera chip would hardly be at the same position with the sample. Thus, only visual adjustment could be done. None of the desired Zn spectral lines were observed in the emission spectra, preventing the determination of LOD.

6.4 Experiment Summary

Two configurations of collecting optics were tested. The optical performance of the system was evaluated based on measurement of a Hg-Ar calibration lamp spectrum. Intensities of specific spectral lines noted in tables 6.3 and 6.4 were compared. The intensity of 253.65 nm Hg line differs by two orders. This result explains why no spectral line of Zn was observed on the wavelength 213.86 nm in any of tyre spectra when using the dichroic mirror configuration. The reflectance of the dichroic mirror for these wavelengths is so low that almost no radiation is collected. However, all results are not according to results expected from simulations. For the last examined Hg spectral line (365.01 nm) the optical performance of the dichroic mirror testing assembly was comparable to the second configuration. It was expected that the intensities gained by the second configurations will be higher throughout the whole wavelength range. However, overal it can be said that the performance of the configuration with two off-axis parabolic mirror is better. It can be seen that the intensity of the Zn I 213.86 spectral line should be the highest of all three desired Zn lines. Thus, the second configuration possibility to effectively collect plasma radiation with lower wavelengths is essential.

Next step was testing both assemblies by measuring solid samples. However, this phase of experiment was complicated by the absence of parabolic mirror with hole used in the second configuration.
The DOF of the dichroic mirror design was determined for the SUS-1 R reference sample. The final value of DOF was DOF = (15.5 ± 0.5) mm. Next, the calibration curve was constructed and LODs of zinc were calculated. The limiting content of Zn that needs to be present in the tyre sample is LOD = (0.75 ± 0.05) %. Although the sensitivity of the system is not very high, it is sufficient for this application. The content of Zn in all tyre samples was determined by XPS method and in all cases was higher than LOD of the LIBS method.

The second testing assembly could not be tested because of absent parabolic mirror. However, testing of optical performance proved both the Zemax simulations and theoretical calculations done in the experimental part. For this reason it can be expected that if tests done with the dichroic mirror configuration would be repeated with this configuration, the results obtained would be better. Because of this, I decided to use the configuration with two parabolic mirrors for my final design of the LIBS module despite all dificulties.

7 Design of the LIBS Module

When designing the optomechanical module, limitations arising from the RoadTrace specification (chapter 4) have to be taken into account. In order to be able to use the mechanism intended for the two-axes linear motion, the mass of the module itself has to be lower than 2 kg. The distance of the lowest point of the module should not be lower than 100 mm.
Apart from these, other requirements for the LIBS module were set:

- optical elements should be fitted so that their optical axes are parallel,
- vertical position of the focusing lens should be adjustable,
- other optical elements should have adjustable pitch and yaw,
- vertical position of the spectrometer should be adjustable,
- electronic components of the spectrometer should be placed on the module.

The conventional way of optomechanical design is assembling optical components into adjustable mounts that are fitted into a cage system. The cage system provides axial alignment of optical elements and also allows their coarse adjustment. However, the cage system could not be used because it is not able to achieve sufficient robustness and because its components are too heavy. Instead, different concept had to be used. The proposed design is shown in Fig. 7.1.

In fig. 7.2, the view on the LIBS module assembly without the cover is shown. A Nd:YAG laser line mirror is mounted in a kinematic mount (1) manufactured by Thorlabs. The focusing lens is in a custom designed mount (2), allowing to adjust its vertical position. The cage (3) with adjustable vertical position holds the primary collecting mirror mount (4) and the secondary collecting mirror mount (5). The spectrometer is placed in a holder (6).

Fig. 7.1: LIBS module assembly. From the outside, base plate and cover are visible. Electronic board of the spectrometer is placed atop the cover.

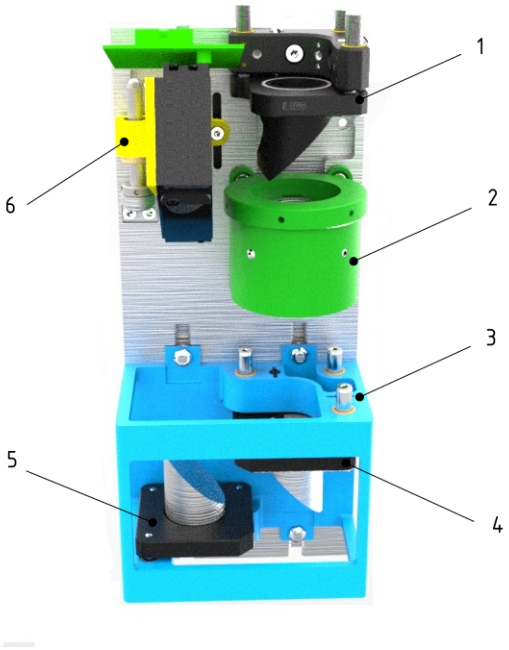

Fig. 7.2: Optomechanical components of the LIBS assembly. 1 - Nd:YAG laserline plane mirrror, 2 - focusing optics mount, 3 - collecting optics cage, 4 - primary parabolic mirror mount, 5 - secondary parabolic mirror mount, 6 - spectrometer holder.

7.1 LIBS Module Components

7.1.1 Base plate

The optomechanical system is placed on an aluminum EN AW 6060 base plate. This material was chosen because it is a relatively cheap and lightweigth metal with good machinability. However, with mass equal to 615 g, this part is the heaviest of the whole assembly. Essential dimensions of the base plate are shown in Fig. 7.3.
Three T-grooves are machined into the base plate. T-grooves in the lower part serve for collecting optics cage adjustment and T-groove in the upper part provides movement of the spectrometer holder.
Apart from ensuring the fitting of all optomechanical components, the plate fastens the module to the robotic unit.

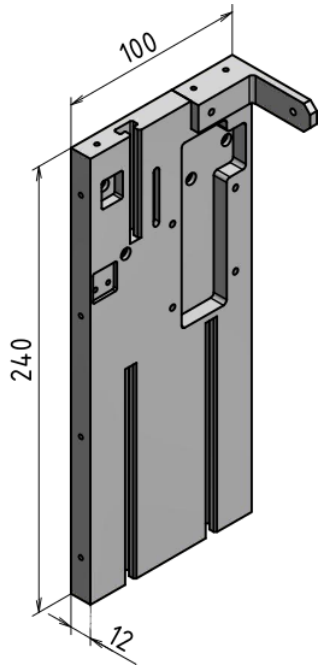

Fig. 7.3: Base plate of the LIBS module. Essential dimensions are marked.

7.1.2 Focusing Optics Mounting

Plane Mirror

The Nd:YAG laserline plane mirror is manufactured by Thorlabs. It has 1" diameter. As was mentioned in chapter 6 of this thesis, this mirror is the last one of plane mirror system guiding the laser pulse into the LIBS module assembly. For this reason, it is necessary that this mirror is adjustable.
The mirror is fitted in commercially available mount manufactured by Thorlabs (see Fig. 7.2). A precision kinematic mirror mount is used. This mount allows 4° pitch and yaw adjustment. The mount is equipped with three screws, allowing to slightly adjust the vertical position of the mirror as well (maximum translation according to the manufacturer is 6.4 mm). The crews can be locked by screw nuts, improving the stability during LIBS module motion. The mount is equipped with two springs. As the LIBS module will be rapidly moving in the horizontal direction, the springs could be a critical component if the resonant frequency was excited by the motion. Because the manufacturer could not provide me with specifications of springs that were used, I simulated them in Ansys software. The mesh sizing was set to 0.2 mm. In the direction of the LIBS module motion, the deformation of the spring is 0.3 mm (see Fig. 7.4). The resonant frequency of the spring is 643.2 Hz. However, the frequency in the horizontal direction due to the movement of the LIBS module is only 7.8 Hz. This means that the spring is stiff enough and its use will not be a limitation. In fact, the use of these springs is unneccessary.

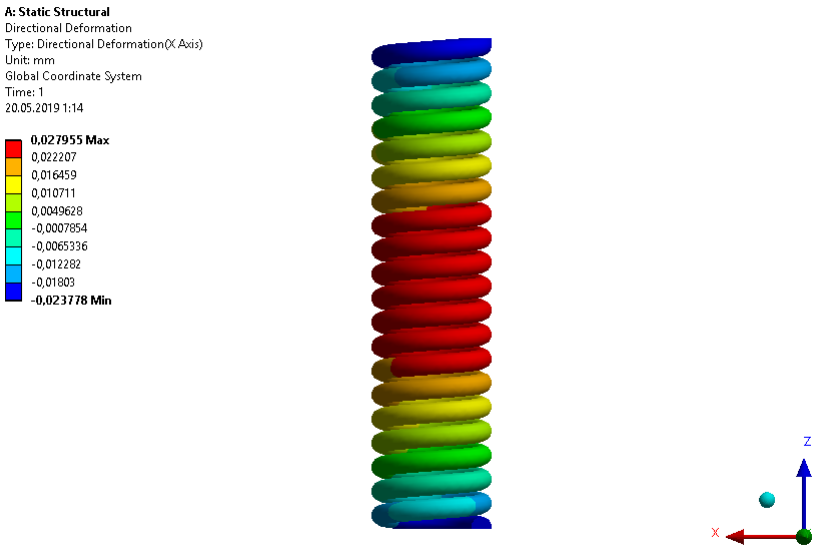

Fig. 7.4: Simulation of the spring deformation in horizontal (x) direction.

Focusing Lens

The focusing lens is mounted in a custom made mount made of aluminum (see Fig. 7.5). Adjusting nut (1) is fitted in a housing (2). The nut is internally threaded (M35x1.5 thread). By rotating the nut in the housing, the position of focusing lens mount (3) changes by the pitch of the thread. The final motion of the lens (4) is linear. Initial position of the lens is defined by two spacers (5) that ensure the position of the lens from both sides. These spacers are made of PTFE (commonly referred to as Teflon), because metal spacers could cause damage to the lens. The motion of the lens is limited by a slot, drilled in the focusing lens mount (3). An ABS stop (6) moves in the slot. Because of feasibility of the design, the slot has to have an "U" shape to be able to insert ABS stops. In order to define a limit position of the linear motion, two M2 set screws (7) are used. The range of the focusing lens mount motion is ±11 mm. Although the adjustment of the lens is coarse (given by the thread pitch 1.5), it is sufficient as it was experimentally proven that DOF of the lens compensates inexactness of the lens distance from the sample.

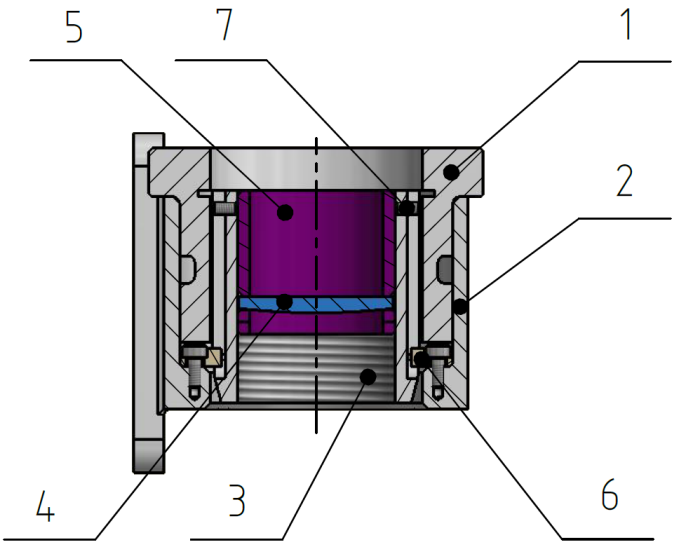

Fig. 7.5: Focusing lens mount. 1 - adjusting nut, 2 - focusing lens mount housing, 3 - focusing lens mount, 4 - focusing lens, 5 - spacers , 6 - ABS stop, 7 - M2 set screw.

7.1.3 Collecting Optics Mounting

Optical elements of the collecting optics are mounted in an aluminum cage (1 in Fig. 7.6). This cage serves as a kinematic mount for both parabolic mirrors. Primary off-axis parabolic mirror (2) is fitted in lower plate of KS1T kinematic mount (3), as well as secondary mirror (4). The kinematic mount has the same properties as the mount chosen for plane mirror in section 7.1.2. However, the upper plate was removed because of weigth reduction. Instead, the upper plate is machined as a part of the cage.

On the back of the cage, two T-grooves are machined, allowing coarse vertical adjustment of the collecting optics in the range ±10 mm. The defined position is then fixed by two clamps in each T-groove. Fine adjustment of both mirrors can be done by adjusting screws on the mirror mounts. Both mounts allow 4° pitch and yaw adjustment and translation in vertical direction by 6.4 mm.

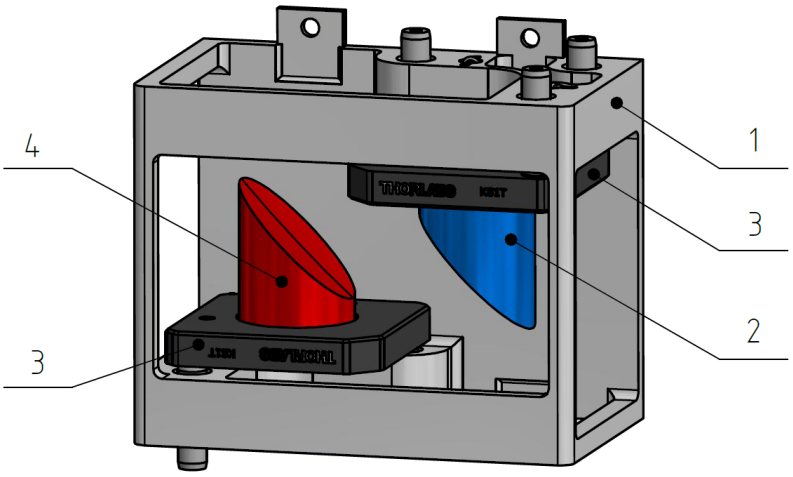

Fig. 7.6: Collecting optics cage mount. 1 - collecting optics cage, 2 - primary parabolic mirror with hole, 3 - lower plate of Thorlabs KS1T mount, 4 - secondary parabolic mirror.

Spectrometer

The spectrometer (1 in Fig. 7.7) is mounted in a custom made aluminum mount (2). The mount has a T-groove machined on its back side, allowing vertical translation without unwanted clearances. The precise adjustment is performed by fine adjustment screw (3) fitted in threaded bushing (4). In order to increase robustness of the adjustment, the position of the screw is secured by a locking nut (5). Fixed connection with the base plate is mediated by a screw housing (6). As can be seen in Fig. 7.2, the position of the mount can be additionaly fixed by a screw moving in a slot. The adjustment range of the spectrometer is ±14 mm.

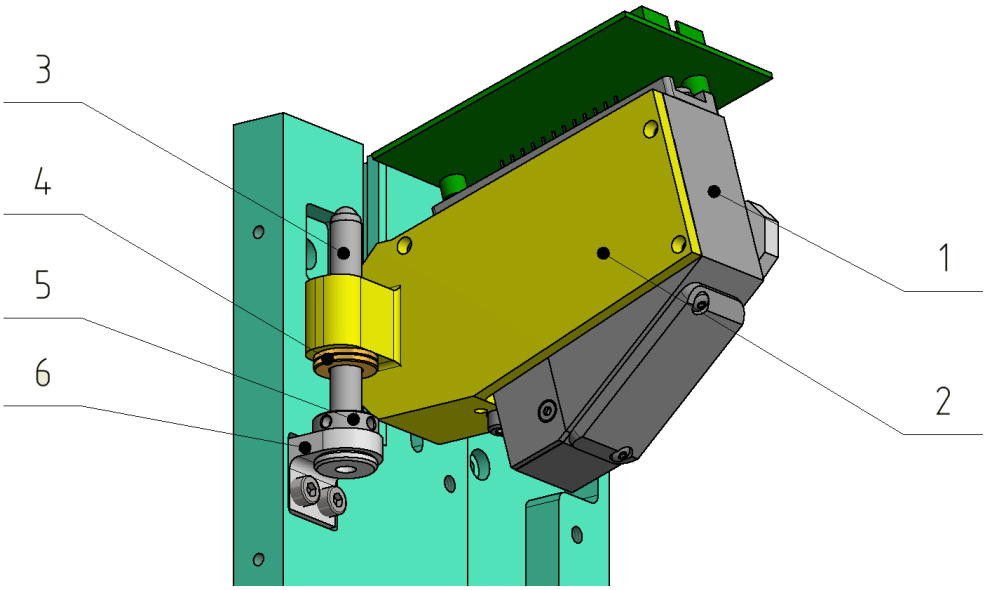

Fig. 7.7: Mount for vertical adjustment of the spectrometer. 1 - spectrometer, 2 - spectrometer mount, 3 - M6x0.25 fine adjustment screw, 4 - threaded bushing, 5 - lock nut, 6 - screw housing.

7.2 Final Design

The LIBS module was assembled partially by manufactured parts and partially by parts purchased from Thorlabs and Edmund Optics companies. All parts that were used for the final design of the LIBS module are listed in the table 7.1. The LIBS module assembly is shown in Fig. 7.8. The most expensive part of the module is the spectrometer, second are manufactured parts. However, the price of the primary parabolic mirror is not listed. The LIBS module was assembled without the primary parabolic mirror. For this reason, it could not be tested at the time of submitting the diploma thesis. Testing of the LIBS module prototype remains for future work.

Tab. 7.1: List of all parts used for the LIBS module prototype.

Item	Vendor	Approx. Price (€)
Purchased parts		
Focusing lens	Thorlabs	77
Secondary parabolic mirror	OptoSigma	N/A
Primary parabolic mirror	Edmund Optics	210
Spectrometer Freedom C-UV	Ibsen Photonics	2920
Optomechanics	Thorlabs	500
Optical windows	Edmund Optics	260
Manufactured parts		
Mechanical parts	Solidcon	2000
3D printed ABS cover	BUT - 3D laboratory	172
	Total price (current):	6139 €

Fig. 7.8: Final prototype of the LIBS module.

8 Conclusion

The aim of this diploma thesis was to design an optomechanical module for chemical mapping using Laser-Induced Breakdown Spectroscopy (LIBS) method. The goals of this thesis could be divided into three parts. First goal was to introduce an appropriate design of focusing and collecting optics. Second goal was to verify the optical design performance with respect to its intended use. Lastly, the chosen optical design was transformed into an optomechanical design of the module.

The first chapter of this diploma thesis briefly introduced the basic physical principles of LIBS method. The LIP formation was described, as well determination of LIP parameters.

Second chapter reviewed the possibilities in remote analysis using LIBS method. Three possible configurations depending on the application were presented – a *portable* LIBS, *remote* LIBS and *stand-off* LIBS configuration. The main focus was given to the last mentioned because this configuration was used in this diploma thesis design.

A brief introduction to braking tracks analysis was presented in the third chapter, followed by the fourth chapter, aiming to introduce the Road-Trace project. Requirements and specifications of the device and the LIBS module itself were presented in this chapter.

Fifth chapter dealt with the optical design. A lens for focusing the plasma pulse on the sample surface was designed based on the input parameters. The depth of field required to be achieved by the focusing lens was 10 mm. A commercially available lens was proposed and its ability to induce plasma on the sample surface was verified.
Three designs of collecting optics were presented. All three designs were simulated in Zemax software, aiming to determine the most efficient one. The efficiency was evaluated based on the amount of plasma radiation that the system was able to transfer to the spectrometer slit. The best results were achieved for a collecting optics design using two off-axis parabolic mirrors.

In chapter 6, the results obtained by simulations of the optical designs in Zemax software were verified. Two optical setups were chosen and compared. Optical performance of the test assemblies was compared with results obtained by theoretical calculation. It was shown that the results are both according these calculations and

the results obtained in Zemax simulations. Tests on solid samples were performed. The depth of field was measured using a standardized sample. The calibration curve was constructed and LODs for Zn were evaluated for the first design. Solid sample measurements could not be performed for the second design because of lack of an essential optical component - the primary parabolic mirror.

The final design of the optomechanical module was presented in chapter 7. First, the module was described as a whole. Then the mounting of focusing and collecting optics was described. This section also contains the pricing of the whole optomechanical module.

The main goal of this diploma thesis – a design of the optomechanical module, was achieved. However, the chemical map of Zn distribution, determining the braking track could not be measured. This goal did not not depend solely on the optomechanical module but also on the design of the robotic unit which was not part of my work. At the time of submitting the diploma thesis, the robotic unit was in the state of initial design. For this reason, evaluating the final design is a matter of future work.

Bibliography

[1] RADZIEMSKI, L. and D. CREMERS. A brief history of laser-induced breakdown spectroscopy: From the concept of atoms to LIBS 2012. *Spectrochimica Acta Part B: Atomic Spectroscopy*, 2013, vol. 47, p. 3-10. DOI: 10.1016/j.sab.2013.05.013. ISSN 05848547. Available from: https://linkinghub.elsevier.com/retrieve/pii/S058485471300116X

[2] LÓPEZ-MORENO, C., PALANCO, S., LASERNA, J., DELUCIA JR, F., MIZIOLEK, A. W., ROSE, J., WALTERS, R. A. and A. I. WHITEHOUSE. Test of a stand-off laser-induced breakdown spectroscopy sensor for the detection of explosive residues on solid surfaces. *Journal of Analytical Atomic Spectrometry*, 2006, vol. 21(1), p. 55-60. DOI: 10.1039/B508055J. ISSN 0267-9477. Available from: http://xlink.rsc.org/?DOI=B508055J

[3] ANGLOS, D., C. BALAS and C. FOTAKIS. Laser spectroscopic and optical imaging techniques in chemical and structural diagnostics of painted artwork. *American Laboratory*, 1999, vol. 31(20), p. 60-67. ISSN 0044-7749.

[4] MARKIEWICZ-KESZYCKA, M., X. CAMA-MONCUNILL, M. P. CASADO-GAVALDA, Y. DIXIT, R. CAMA-MONCUNILL, P. J. CULLEN and C. SULLIVAN. Laser-induced breakdown spectroscopy (LIBS) for food analysis: A review. *Trends in Food Science & Technology*, 1999, vol. 65, p. 80-93. DOI: 10.1016/j.tifs.2017.05.005. ISSN 09242244. Available from: https://linkinghub.elsevier.com/retrieve/pii/S0924224417300377

[5] NOLL, R., C. FRICKE-BEGEMANN, M. BRUNK, et al. Laser-induced breakdown spectroscopy expands into industrial applications. *Spectrochimica Acta Part B: Atomic Spectroscopy*, 2014, vol. 93, p. 41-51. DOI: 10.1016/j.sab.2014.02.001. ISSN 05848547. Available from: https://linkinghub.elsevier.com/retrieve/pii/S0584854714000160

[6] PROCHAZKA, D., M. BILÍK, P. PROCHAZKOVA, et al. Detection of visually unrecognizable braking tracks using Laser-Induced Breakdown Spectroscopy, a feasibility study. *Spectrochimica Acta Part B: Atomic Spectroscopy*, 2016, vol. 118, p. 90-97. DOI: 10.1016/j.sab.2016.02.013. ISSN 05848547. Available from: https://linkinghub.elsevier.com/retrieve/pii/S0584854716300040

[7] VITTIGLIO, G., K. JANSSENS, B. VEKEMANS, F. ADAMS and A. OOST. A compact small-beam XRF instrument for in-situ analysis of objects of historical and/or artistic value. *Spectrochimica Acta Part B: Atomic Spectroscopy*, 1999, vol. 54(12), p. 1697-1710. DOI: 10.1016/S0584-8547(99)00100-7. ISSN 05848547. Available from: https://linkinghub.elsevier.com/retrieve/pii/S0584854799001007

[8] VANDENABEELE, P., K. CASTRO, M. HARGREAVES, L. MOENS, J.M. MADARIAGA and H.G.M. EDWARDS. Comparative study of mobile Raman instrumentation for art analysis. *Analytica Chimica Acta*, 2007, vol. 588(1), p. 108-116. DOI: 10.1016/j.aca.2007.01.082. ISSN 00032670. Available from: https://linkinghub.elsevier.com/retrieve/pii/S0003267007002656

[9] SNYDER, A. P., SHOFF, D. B., EICEMAN G. A., BLYTH, D. A. and J. A. PARSONS. Detection of bacteria by ion mobility spectrometry. *Analytical Chemistry*, 2002, vol. 63(5), p. 526-529. DOI: 10.1021/ac00005a028. ISSN 0003-2700. Available from: http://pubs.acs.org/doi/abs/10.1021/ac00005a028

[10] FORTES, F.J. and J.J. LASERNA. The development of fieldable laser-induced breakdown spectrometer: No limits on the horizon. *Spectrochimica Acta Part B: Atomic Spectroscopy*, 2010, vol. 65(12), p. 975-990. DOI: 10.1016/j.sab.2010.11.009. ISSN 05848547. Available from: https://linkinghub.elsevier.com/retrieve/pii/S058485471000296X

[11] RAKOVSKY, J., P. CERMAK, O. MUSSET and P. VEIS. A review of the development of portable laser induced breakdown spectroscopy and its applications. *Spectrochimica Acta Part B: Atomic Spectroscopy*, 2014, vol. 101, p. 269-287. DOI: 10.1016/j.sab.2014.09.015. ISSN 05848547. Available from: https://linkinghub.elsevier.com/retrieve/pii/S0584854714002663

[12] PROCHAZKA, D. *Detekce brzdných stop pomocí spektrometrie laserem indukovaného plazmatu (LIBS) a spektrometrie laserem indukované fluorescence (LIBS+LIFS).* [Doctoral Thesis]. Brno: VUT, FSI, 2014, 97 p.

[13] PROCHAZKA, D., M. BILIK, P. PROCHAZKOVA, et al. Detection of tire tread particles using laser-induced breakdown spectroscopy. *Spectrochimica Acta Part B: Atomic Spectroscopy*, 2015, vol. 108, p. 1-7. DOI: 10.1016/j.sab.2015.03.011. ISSN 05848547. Available from: https://linkinghub.elsevier.com/retrieve/pii/S0584854715000853

[14] LIBS - Laser-Induced Breakdown Spectroscopy. *Laser spectroscopy - Ceitec.cz* [online]. [cit. 2019-05-08] Available from: http://libs.ceitec.cz/libs-laser-induced-breakdown-spectroscopy/

[15] HAHN, D. W. and N. OMENETTO. Laser-Induced Breakdown Spectroscopy (LIBS), Part II: Review of Instrumental and Methodological Approaches to Material Analysis and Applications to Different Fields. *Applied Spectroscopy*, 2012, vol. 66(4), p. 347-419. DOI: 10.1366/11-06574. ISSN 0003-7028. Available from: http://journals.sagepub.com/doi/10.1366/11-06574

[16] NOLL, R. *Laser-Induced Breakdown Spectroscopy: Fundamentals and Applications.* Berlin, D: Springer, 2012. ISBN 978-3-642-20667-2.

[17] PORIZKA, P. *Using Laser-induced Breakdown Spectroscopy (LIBS) for Material Analysis.* [Doctoral Thesis]. Brno: VUT, FSI, 2014, 115 p.

[18] NOVOTNY, J. *Dálkově řízená laserová spektroskopie (LIBS).* [Doctoral Thesis]. Brno: VUT, FSI, 2014, 97 p.

[19] *Handbook of solid-state lasers: materials, systems and applications* [online]. Philadelphia, PA: Woodhead Publishing, 2013 [cit. 2019-05-08]. ISBN 08-570-9272-3. Available from: https://doi.org/10.1533/9780857097507.2.551

[20] CREMERS, D. A. and L. J. RADZIEMSKI. *Handbook of laser-induced breakdown spectroscopy.* Hoboken, NJ: John Wiley, 2006. ISBN 04-700-9299-8.

[21] HAHN, D. W. and N. OMENETTO. Laser-Induced Breakdown Spectroscopy (LIBS), Part I: Review of Basic Diagnostics and Plasma—Particle Interactions. *Applied Spectroscopy*, 2010, vol. 64(12), p. 335A-366A. DOI: 10.1366/000370210793561691. ISSN 0003-7028. Available from: http://journals.sagepub.com/doi/10.1366/000370210793561691

[22] CRISTOFORETTI, G., A. DE GIACOMO, M. DELL'AGLIO, S. LEGNAIOLI, E. TOGNONI, V. PALLESCHI, and N. OMENETTO. Local Thermodynamic Equilibrium in Laser-Induced Breakdown Spectroscopy: Beyond the McWhirter criterion. *Spectrochimica Acta Part B: Atomic Spectroscopy*, 2010, vol. 65(1), p. 86-95. DOI: 10.1016/j.sab.2009.11.005. ISSN 05848547. Available from: https://linkinghub.elsevier.com/retrieve/pii/S0584854709003541

[23] BROEKAERT, J. A. C. *Analytical atomic spectrometry with flames and plasmas.* 2nd completely rev. and extended ed. Chichester: John Wiley, 2005. ISBN 978-352-7312-825.

[24] PseudoVoigt. *Mantid Project* [online]. [cit. 2019-05-08] Available from: https://docs.mantidproject.org/nightly/fitting/fitfunctions/PseudoVoigt.html

[25] TOGNONI, E., G. CRISTOFORETTI, S. LEGNAIOLI, V. PALLESCHI, A. SALVETTI, M. MUELLER, U. PANNE and I. GORNUSHKIN. A numerical study of expected accuracy and precision in Calibration-Free Laser-Induced Breakdown Spectroscopy in the assumption of ideal analytical plasma. *Spectrochimica Acta Part B: Atomic Spectroscopy*, 2007, vol. 62(12), p. 1287-1302. DOI: 10.1016/j.sab.2007.10.005. ISSN 05848547. Available from: https://linkinghub.elsevier.com/retrieve/pii/S0584854707003187

[26] MIZIOLEK, A. W., V. PALLESCHI and I. SCHECHTER. *Laser-induced Breakdown Spectroscopy (LIBS): Fundamentals and Applications.* Cambridge, UK: Cambridge University Press, 2006. ISBN 0-521-85274-9.

[27] DUDRAGNE, L., Ph. ADAM and J. AMOUROUX. Time-Resolved Laser-Induced Breakdown Spectroscopy: Application for Qualitative and Quantitative Detection of Fluorine, Chlorine, Sulfur, and Carbon in Air. *Applied Spectroscopy*, 2016, vol. 52(10), p. 1321-1327. DOI: 10.1366/0003702981942654. ISSN 0003-7028. Available from: http://journals.sagepub.com/doi/10.1366/0003702981942654

[28] Atomic Spectra Database. *NIST* [online]. [cit. 2019-05-08] Available from: https://www.nist.gov/pml/atomic-spectra-database

[29] *AtomAnalyzer* [online]. [cit. 2019-05-08] Available from: https://atomanalyzer.com/

[30] MYERS, M. J., W. A. CLARKSON, N. HODGSON, et al. LIBS system with compact fiber spectrometer, head mounted spectra display and hand held eye-safe erbium glass laser gun. *Solid State Lasers XIX: Technology and Devices Conference*, 2010, vol. p. 7578-7587. DOI: 10.1117/12.841901. Available from: http://proceedings.spiedigitallibrary.org/proceeding.aspx?doi=10.1117/12.841901

[31] YAMAMOTO, K. Y., D. A. CREMERS, M. J. FERRIS and L. E. FOSTER. Detection of Metals in the Environment Using a Portable Laser-Induced Breakdown Spectroscopy Instrument. *Applied Spectroscopy*, 1996, vol. 50(2), p. 222-233. DOI: 10.1366/0003702963906519. ISSN 0003-7028. Available from: http://journals.sagepub.com/doi/10.1366/0003702963906519

[32] DONA-FERNANDEZ, A., I. DE ANDRES-GIMENO, P. SANTIAGO-TORIBIO, E. VALTUILLE-FERNANDEZ, F. ALLER-SANCHEZ and A. HERAS-GONZALEZ. Real-time detection of GSR particles from crime scene: A comparative study of SEM/EDX and portable LIBS system. *Forensic Science International*, 2018, vol. 292, p. 167-175. DOI: 10.1016/j.forsciint.2018.09.021. ISSN 03790738. Available from: `https://linkinghub.elsevier.com/retrieve/pii/S0379073818308120`

[33] WHITEHOUSE, A.I., J. YOUNG, I.M. BOTHEROYD, S. LAWSON, C.P. EVANS and J. WRIGHT. Remote material analysis of nuclear power station steam generator tubes by laser-induced breakdown spectroscopy. *Spectrochimica Acta Part B: Atomic Spectroscopy*, 2001, vol. 56(6), p. 821-830. DOI: 10.1016/S0584-8547(01)00232-4. ISSN 05848547. Available from: `https://linkinghub.elsevier.com/retrieve/pii/S0584854701002324`

[34] PALANCO, S. and J. J. LASERNA. Full automation of a laser-induced breakdown spectrometer for quality assessment in the steel industry with sample handling, surface preparation and quantitative analysis capabilities. *Journal of Analytical Atomic Spectrometry*, 2000, vol. 15(10), p. 1321-1327. DOI: 10.1039/b003632n. ISSN 02679477. Available from: `http://xlink.rsc.org/?DOI=b003632n`

[35] RAI, A. K., H. ZHANG, F. Y. YUEH, J. P. SINGH and A. WEISBERG. Parametric study of a fiber-optic laser-induced breakdown spectroscopy probe for analysis of aluminum alloys. *Spectrochimica Acta Part B: Atomic Spectroscopy*, 2001, vol. 56(12), p. 2371-2383 .DOI: 10.1016/S0584-8547(01)00299-3. ISSN 05848547. Available from: `https://linkinghub.elsevier.com/retrieve/pii/S0584854701002993`

[36] CREMERS, D. A., J. E. BAREFIELD and A. C. KOSKELO. Remote Elemental Analysis by Laser-Induced Breakdown Spectroscopy Using a Fiber-Optic Cable. *Applied Spectroscopy*, 2016, vol. 49(6), p. 857-860. DOI: 10.1366/0003702953964589. ISSN 0003-7028. Available from: `http://journals.sagepub.com/doi/10.1366/0003702953964589`

[37] SALLÉ, B., P. MAUCHIEN and S. MAURICE. Laser-Induced Breakdown Spectroscopy in open-path configuration for the analysis of distant objects. *Spectrochimica Acta Part B: Atomic Spectroscopy*, 2007, vol. 62(8), p. 739-768. DOI: 10.1016/j.sab.2007.07.001. ISSN 05848547. Available from: `https://linkinghub.elsevier.com/retrieve/pii/S0584854707001929`

[38] MAURICE, S., R. C. WIENS, M. SACCOCCIO, et al. The ChemCam Instrument Suite on the Mars Science Laboratory (MSL) Rover: Science Objectives and Mast Unit Description. *Space Science Reviews*, 2012, vol. 170(1-4), p. 95-166. DOI: 10.1007/s11214-012-9912-2. ISSN 0038-6308. Available from: http://link.springer.com/10.1007/s11214-012-9912-2

[39] BORN, M. and E. WOLF. *Principles of Optics. Electromagnetic Theory of Propagation, Interference and Diffraction of Light.* Cambridge, UK: Cambridge University Press, 1997. ISBN 0-521-63921-2.

[40] NEUHAUSER, R. E., U. PANNE and R. NIESSNER. Utilization of Fiber Optics for Remote Sensing by Laser-Induced Plasma Spectroscopy (LIPS). *Applied Spectroscopy*, 2000, vol. 54(6), p. 923-927. DOI: 10.1366/0003702001950337. ISSN 0003-7028. Available from: http://journals.sagepub.com/doi/10.1366/0003702001950337

[41] LASERNA, J.J., R. F. REYES, R. GONZÁLEZ, L. TOBARIA and P. LUCENA. Study on the effect of beam propagation through atmospheric turbulence on standoff nanosecond laser induced breakdown spectroscopy measurements. *Optics Express*, 2009, vol. 17(12), p. 10265-10276. DOI: 10.1364/OE.17.010265. ISSN 1094-4087. Available from: https://www.osapublishing.org/oe/abstract.cfm?uri=oe-17-12-10265

[42] FAUSER, P., J. C. TJELL, H. MOSBAEK and K. PILEGAARD. Quantification of Tire-Tread Particles Using Extractable Organic Zinc as Tracer. *Rubber Chemistry and Technology*, 1999, vol. 72(5), p. 969-977. DOI: 10.5254/1.3538846. ISSN 0035-9475. Available from: http://rubberchemtechnol.org/doi/abs/10.5254/1.3538846

[43] SALEH, B. E. A. and M. C. TEICH. *Fundamentals of Photonics.* 2nd ed. Hoboken: Wiley-Interscience, 2007. ISBN 978-0-471-35832-9.

[44] O. SVELTO. *Principles of Lasers.* 5th ed. New York: Springer, 2010. ISBN 978-1-4419-1301-2.

[45] M. J. REIDL. *Optical Design Fundamentals for Infrared Systems* 2nd ed. Washington: Spie Press, 2001. 0-8194-4051-5.

[46] *Thorlabs, Inc.* [online]. [cit. 2019-05-08] Available from: https://www.thorlabs.com/

[47] Freedom UV *Ibsen Photonics* [online]. [cit. 2019-05-08] Available from: https://ibsen.com/products/oem-spectrometers/freedom-spectrometers/freedom-uv/

[48] X-ray Photoelectron Spectroscopy Kratos Axis Supra *CEITEC Nano* [online]. [cit. 2019-05-18] Available from: `http://nano.ceitec.cz/x-ray-photoelectron-spectroscopy-kratos-axis-supra/`

[49] GLÉZL, S, J. KAMARÁD and I. SLIMÁK. *Presná mechanika.* Bratislava: Vydavatelstvo Alfa, 1992. ISBN 80-05-00972-0.

[50] Z. HARNA. *Přesná mechanika.* Brno: VUT, 1996. ISBN 80-214-0794-8.

[51] J. LEINVEBER and P. VÁVRA. *Strojnické tabulky.* 2nd ed. Úvaly: Pedagogické nakladatelství, 2005. ISBN 80-7361-011-6.

[52] SHIGLEY, J. E., C. R. MISCHKE and R. G. BUDYNAS. *Konstruování strojních součástí.* Brno: VUTIUM, 2010. ISBN 978-80-214-2629-0.

List of symbols, physical constants and abbreviations

n_c	critical electron density
λ	wavelength
n_e	electron density
T	temperature
ΔE_{nm}	energy difference between energy levels n and m
Δt	lifetime of an energy state
E	energy
h	Planck constant
n_k^s	population density of species s in excited quantum states on level k
n^s	total number density of species s
g_k	statistical weight
U_s	internal partition function
E_k	excitation energy of level k
k_B	Boltzmann constant
I_λ^{ki}	integral density of an optically thin emission line of wavelength λ
A_{ki}	transition probability (Einstein coefficient)
$\Delta\lambda_{Stark}$	Stark broadening of an emission line
w_e	electron impact half-width
s_B	standard deviation of the signal background
S	sensitivity of the calibration curve
M^2	quality factor of the Gaussian beam
r	distance from the sample
D	laser beam diameter in the principal plane of focusing lens
g	gravitational constant
f	focal length
z_0	Rayleigh distance
w'	waist radius (minimum radius of the Gaussian beam)
R	radius of curvature
LIBS	Laser-induced Breakdown Spectroscopy
GC-MS	Gas Chromatography - Mass Spectrometry
XRF	X-ray Fluorescence
IMS	Ion Mobility Spectrometry
LIF	Laser-Induced Fluorescence
CCD	Charge-coupled device
ICCD	Intensified charge-coupled device

LIP	Laser-induced Plasma
LTE	Local Thermodynamic Equilibrium
FWHM	Full Width at Half Maximum
SNR	Signal to Noise Ratio
NIST	National Institute of Standards and Technology
LOD	Limits of Detection
SEM	Scanning Electron Microscope
EDX	Energy Dispersive X-ray Spectroscopy
NA	Numeric Aperture
DOF	Depth of Field
MSL	Mars Science Laboratory
ABS	Anti-lock braking
CEITEC	Central European Institute of Technology
LGP	Light Gathering Power

List of appendices

A Results of DOF Measurements

A.1 Results for Configuration with Dichroic Mirror

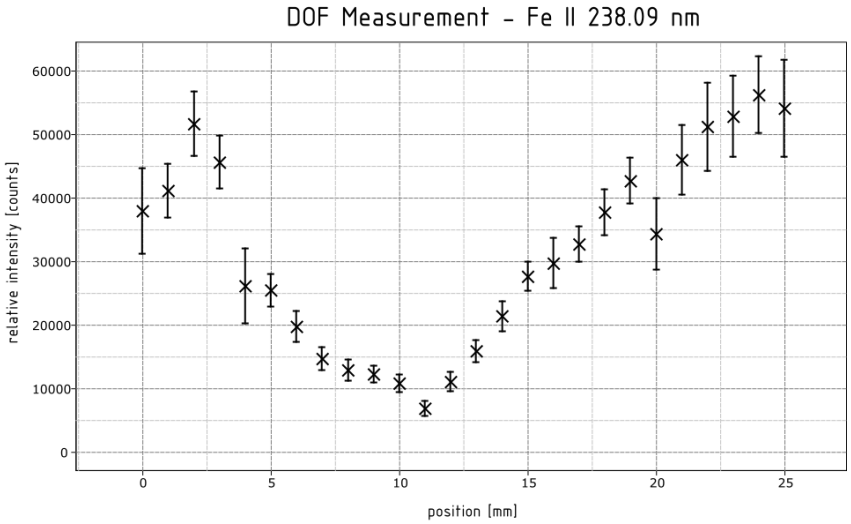

Fig. A.1: DOF measurement for a wavelength interval around Fe II 238.09 nm spectral line. The DOF cannot be determined from this measurement. Zero on the x axis marks the position farthest from the focusing lens.

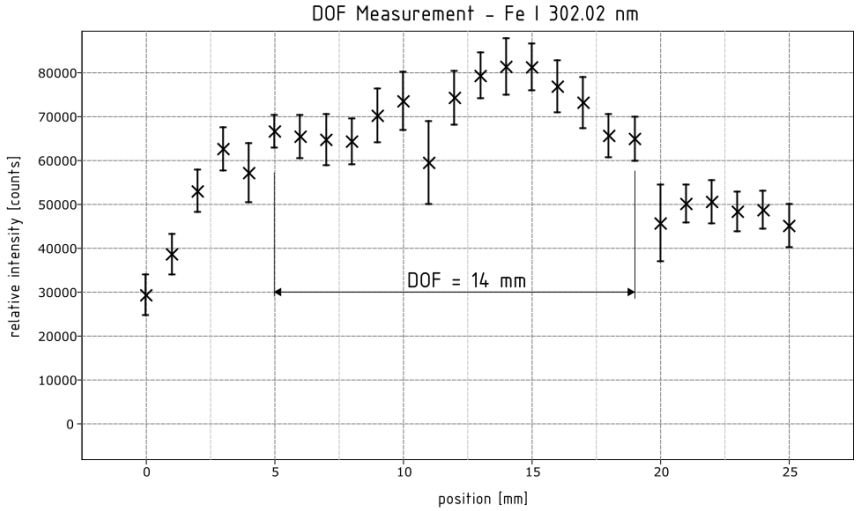

Fig. A.2: DOF measurement for a wavelength interval around Fe I 302.02 nm spectral line. The DOF determined for this wavelength is 14 mm. Zero on the x axis marks the position farthest from the focusing lens.

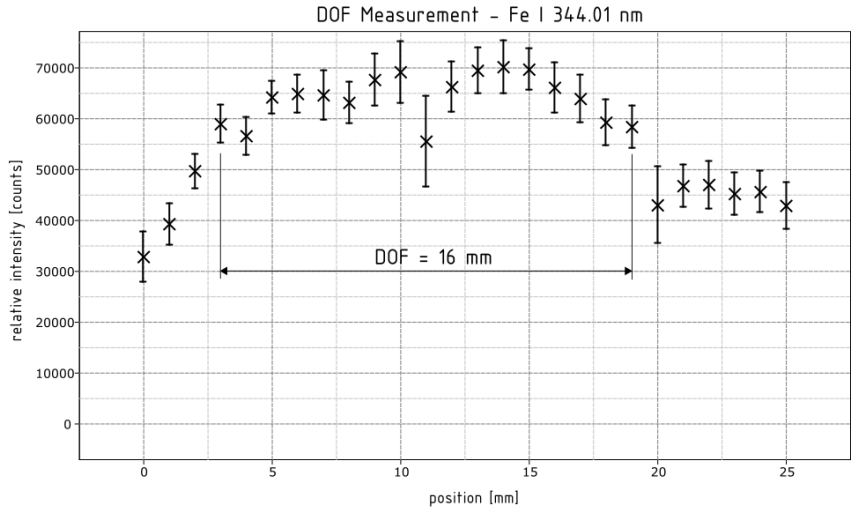

Fig. A.3: DOF measurement for a wavelength interval around Fe I 344.01 nm spectral line. The DOF determined for this wavelength is 16 mm. Zero on the x axis marks the position farthest from the focusing lens.

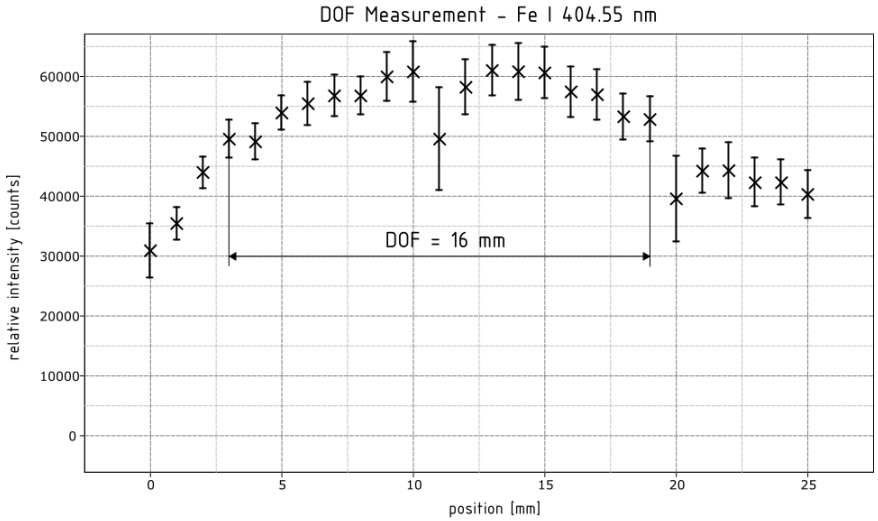

Fig. A.4: DOF measurement for a wavelength interval around Fe I 404.55 nm spectral line. The DOF determined for this wavelength is 16 mm. Zero on the x axis marks the position farthest from the focusing lens.

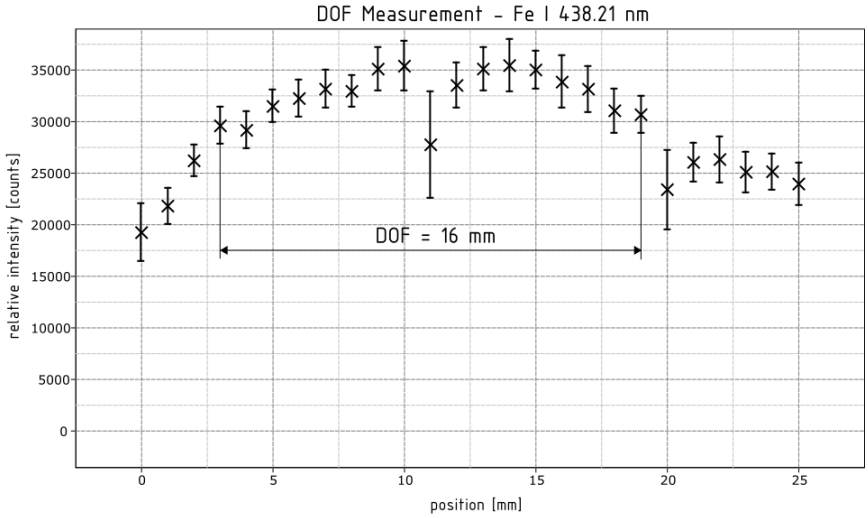

Fig. A.5: DOF measurement for a wavelength interval around Fe I 438.21 nm spectral line. The DOF determined for this wavelength is 16 mm. Zero on the x axis marks the position farthest from the focusing lens.

B List of Technical Documentation

Title	Part Number	Sheet Size
UCHYT SPEKTROMETRU	D_01	A2
DRZAK POSUVU COCKY	D_02	A3
POSUV COCKY VNEJSI	D_03	A4
POSUV COCKY VNITRNI	D_04	A4
DISTANCE	D_05	A4
DISTANCE	D_06	A4
CEP	D_07	A4
HOUSING	D_08	A4
DESKA	D_09	A3
KOSTKA	D_10	A4
KLEC SBERNE OPTIKY	D_11	A2
NOSNA DESKA MODULU	D_12	A2
INSERT	D_13	A4